

Nansen Environmental and Remote Sensing Center

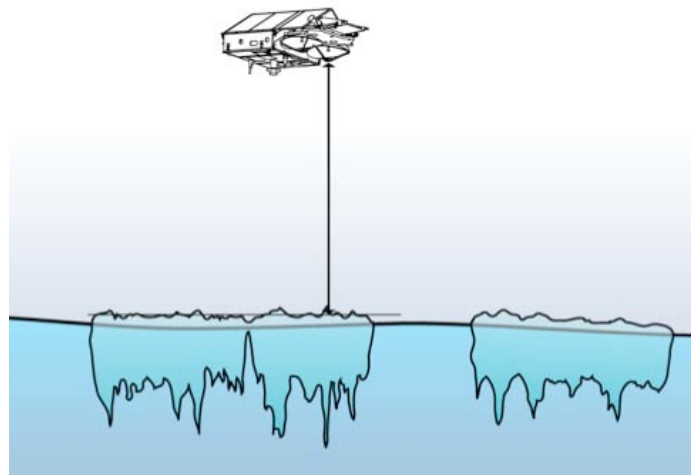


NERSC Technical Report no. 320

CryoSat sea ice validation and process studies in the European Arctic

2008 - 2010


PRODEX contract No. C90318



February 2011

Investigators:

*Stein Sandven, Kjell Kloster, Marta Zygmuntowska, Johan Wåhlin, Sebastian Gerland,
Sanja Forsström and Frank Nilsen*

	<p align="center">Nansen Environmental and Remote Sensing Center (NERSC)</p> <p align="right">Thormøhlensgate 47 N-5006 Bergen, Norway Phone: + 47 55 20 58 00 Fax: + 47 55 20 58 01 E-Mail: Stein.Sandven@nersc.no http://www.nersc.no</p>
---	--

<p>TITLE: CryoSat sea ice validation and process studies in the European Arctic</p> <p>Final report</p>	<p>REPORT IDENTIFICATION</p> <p>NERSC Technical report no. 320</p>
<p>CLIENT ESA PRODEX</p>	<p>CONTRACT PRODEX contract No. C90318</p>
<p>CLIENT REFERENCE Malcolm Davidson</p>	<p>AVAILABILITY Customer report</p>
<p>INVESTIGATORS</p> <p>Stein Sandven (NERSC) Kjell Kloster (NERSC) Marta Zygmuntowska (NERSC) Johan Wåhlin (NERSC) Sebastian Gerland (NPI) Sanja Forsström (NPI) Frank Nilsen (UNIS)</p>	<p>AUTHORISATION</p> <p>Final report 28 February 2011</p> <p>Stein Sandven</p>

Contents

EXECUTIVE SUMMARY	2
WP1 REPORT ON SEA ICE AND SNOW STATISTICS FROM HISTORICAL DATA	3
WP2: REPORT ON RADAR AND LASER DATA FROM AIRBORNE CAMPAIGNS	11
THE AIRBORNE CAMPAIGN IN 2006	11
ASIRAS DATA FROM 02 MAY 2006	12
THE AIRBORNE CAMPAIGN IN 2008	14
WP3: REPORT ON SEA ICE DATA FROM IPY PROJECTS	23
DATA COLLECTION BY UNIS IN 2008 – 2009	23
DATA COLLECTED BY UNIS IN 2010 USING A GEONICS EM-31 INSTRUMENT.....	25
DATA COLLECTION BY NPI	32
WP4: REPORT ON ICESAT DATA ANALYSIS	39
USE OF ICESAT ALTIMETER DATA FOR SEA ICE THICKNESS RETRIEVAL.....	39
FIRST LOOK AT CRYOSAT DATA	43
WP5: PLAN FOR POST-LAUNCH EXPERIMENTS	43
WP6: WORKSHOP/CONFERENCE ON CRYOSAT2 SEA ICE DATA	45
REFERENCES	45
APPENDIX: PROCESSING OF ASIRAS AND ALS DATA	48
A1. ASIRAS 2008 REPROCESSED DATA PROCESSING	48
A2. ALS 2008 DATA PROCESSING	49

Executive Summary

The project has focused on analysis of sea ice physics data from previous and new field expeditions in order to establish the relationship between freeboard, snow cover, snow & ice density and snow & ice thickness. This relationship is the basis for the ice thickness retrieval algorithm for CryoSat-2. This algorithm needs to be adjusted and validated for different regions and months of the year using available data from in situ field experiments and airborne campaigns. Historical data on ice and snow properties have been analysed to improve the regional and seasonal statistics of snow thickness, ice density and other key parameters needed to validate the altimeter retrievals. Field investigations have been conducted in the Svalbard region and the Fram Strait to obtain in situ measurements of ice thickness, freeboard, density and snow properties. Data from these investigations have been analysed and presented in the report. Examples of airborne radar (ASIRAS) and laser data (ALS) from the previous CryoVex 2006 and 2008 campaigns have been analysed to study the return signals from different ice and snow surfaces. Radar and laser altimeter signals have different reflections from the surface. Laser altimeter signals are reflected from the snow surface, while radar altimeter signals are in principle reflected from the snow-ice interface (as long as the snow is dry). Both radar and laser altimeter data can be used to measure freeboard and convert freeboard to thickness. By combining high-resolution altimeter profiles with scanning laser data and SAR images, it is possible to separate leads with open water or thin ice from thick ice floes with ridges. Examples of waveform data from ASIRAS covering different ice types have been presented. Satellite laser altimeter data from IceSat have been obtained for selected periods from 2003 to 2008 and analyzed for the Fram Strait area, where surface roughness and ice freeboard and thickness have been retrieved. The first examples of CyoSat level 1b data have been obtained over sea ice in the Fram Strait, but results are not yet available. Results of the project have been published in journals and presented at conferences and workshops. Finally, plans for participation in the CryoSat post-launch calval experiment in 2011 (CryoVex 2011) have been prepared.

The project consisted of the following six workpackages:

- WP1: Sea ice and snow statistics from historical data
- WP2: Analysis of radar and laser data from airborne campaigns
- WP3: Analysis of sea ice data from recent field investigations
- WP4: IceSat data analysis examples in the Fram Strait
- WP5: Plan for post-launch experiment
- WP6: Workshop/conference on CryoSat-2 sea ice data.

The results of the work in each of the workpackages are presented in this report.

WP1 Report on sea ice and snow statistics from historical data

WP1: Compile and analyze historical snow and sea ice physics data, including use of Russian archives, to determine seasonal and regional statistics of thickness, freeboard, snow cover, and density.

One of the most extensive observing programmes for sea ice and snow measurements in the Arctic Ocean was the Sever expeditions from 1928 to 1989 (NSIDC, 2004; Alexandrov et al., 2010). The Sever data set consists of raw data files from 3771 aircraft landings which took place mainly from mid March to early May. Sea ice thickness, freeboard, snow depth, as well as several other ice parameters were measured. Ice thickness was measured at 3-5 locations 150-200 m apart on the runway, and, when second-year and multiyear ice prevailed in the landing area, at 10-20 points on the neighboring ice floes and at fresh fractures. The obtained values were averaged and used for analysis and presented in the ice and snow atlas by [Romanov, 1995]. Snow depth was measured at 10-20 random points over the entire ice floe, and on adjacent floes, as well as at 3-5 points on the runway on level first-year and, whenever possible, on multiyear ice. Other data collected in the Sever expeditions includes floe size, snow depth, size of ridges and hummocks, sastrugi size and area, snow density and ice freeboard.

An overview of the location and temporal distribution of the data are presented in Fig. 1.1 and Table 1.1. Examples of geographical distribution of measurements are shown in Fig. 1.2. A subset of the data are presented in Table 1.2 where both ice thickness freeboard, as well as snow depth were measured in 689 landings in the period February-May of 1980-1982, 1984-1986, and 1988.

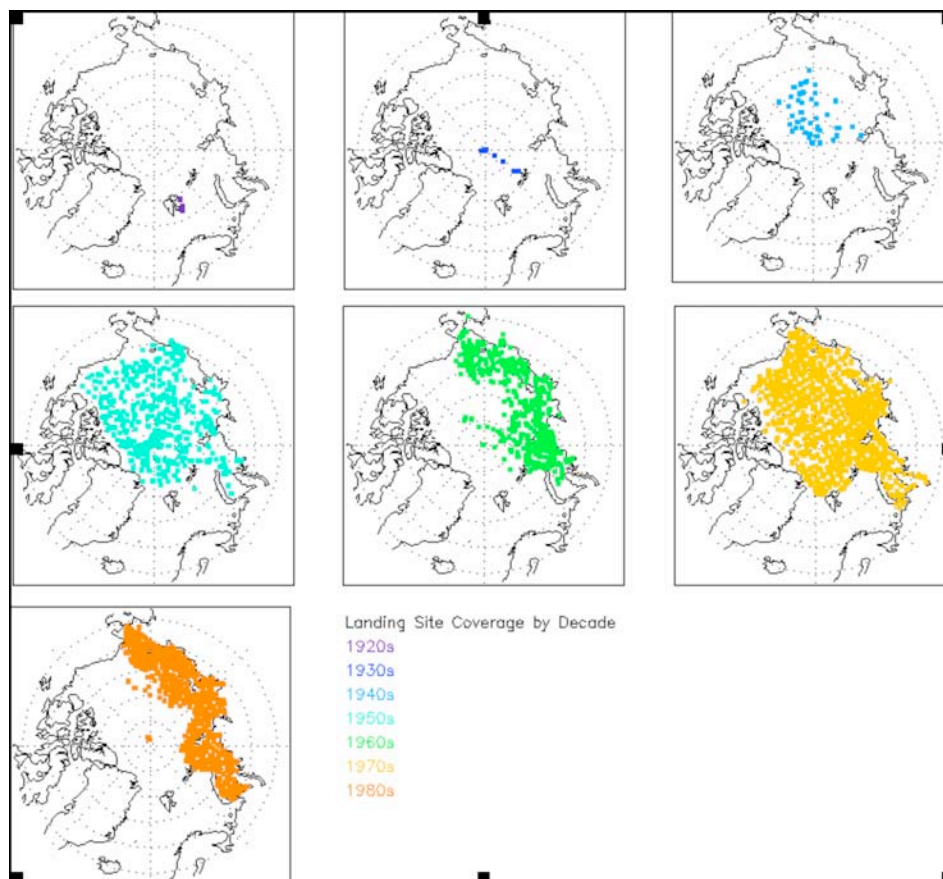


Figure 1.1. Landing sites of the Sever expeditions for each decade

Table 1.1: Number of landing sites per area for each decade

	Eastern Arctic	Western Arctic	Fram Strait	Barents Sea	Kara Sea	Laptev Sea	East Siberian Sea	Chukchi Sea	Beaufort Sea
1920s				4					
1930s	6	1							
1940s	8	35			1	1			
1950s	85	183		3	26	56	80	8	20
1960s	39	31			302	216	90	57	
1970s	232	349	14	26	170	215	94	116	42
1980s	12	93		28	315	329	251	198	
Total	382	692	14	61	814	817	515	379	62

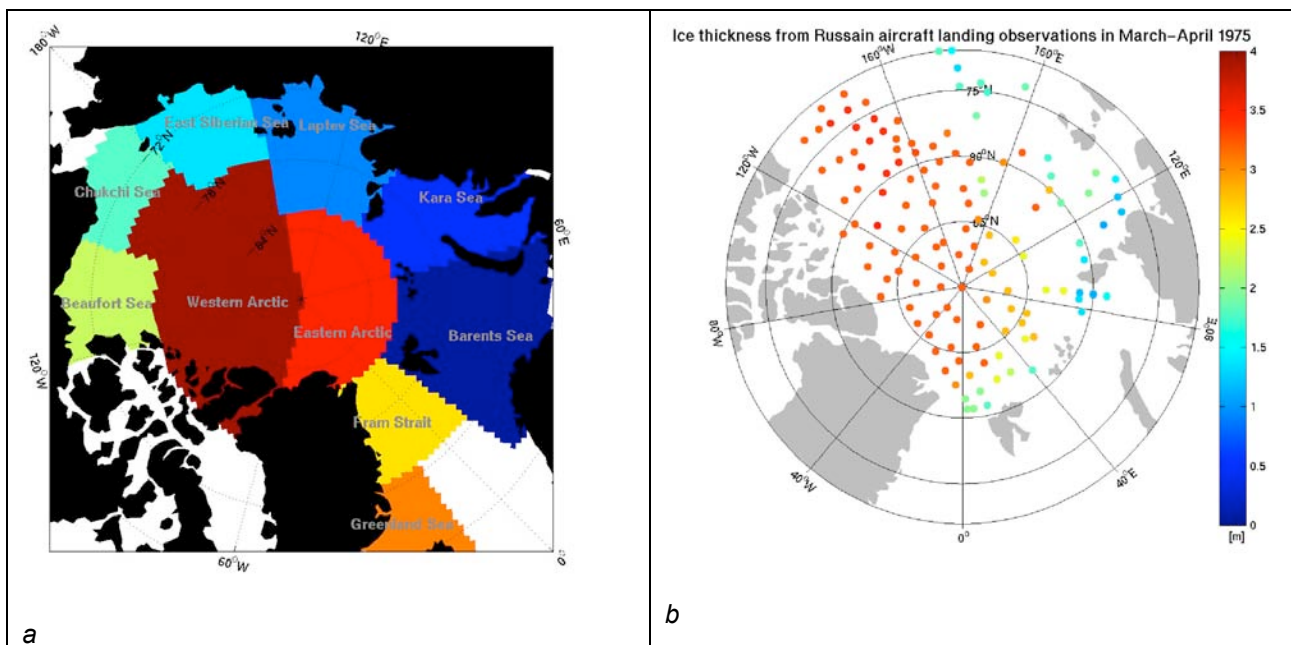


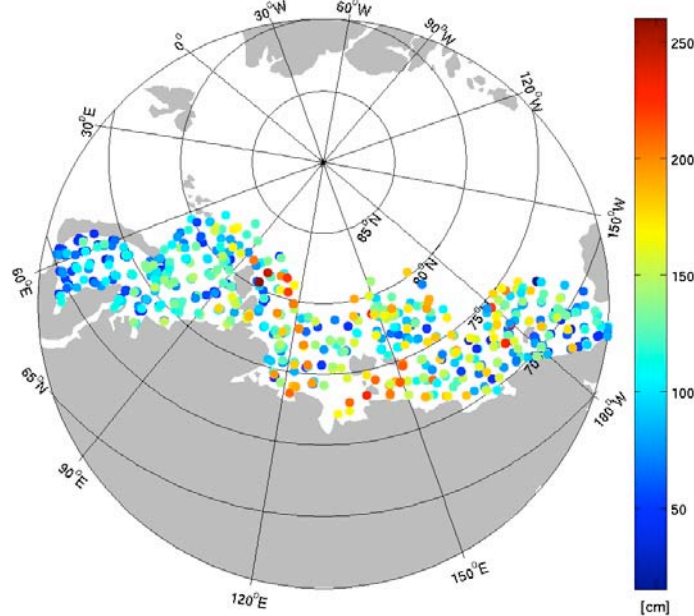
Figure 1.2: (a) Regions where ice thickness and other Sever data were collected; (b) example of thickness data collected during March and April 1975 with the mean thickness at each site indicated in colours.

Table 1.2. Temporal distribution of ice thickness/freeboard and snow depth measurements used for analysis of the relation between ice thickness and ice freeboard.

	February	March	April	May	Total
1980		48	65	18	131
1981		3	10	8	21
1982		28	34	24	86
1984	2	33	57	36	128
1985		46	57	61	164
1986		25	74	51	150
1988			9		9
Total	2	183	306	198	689

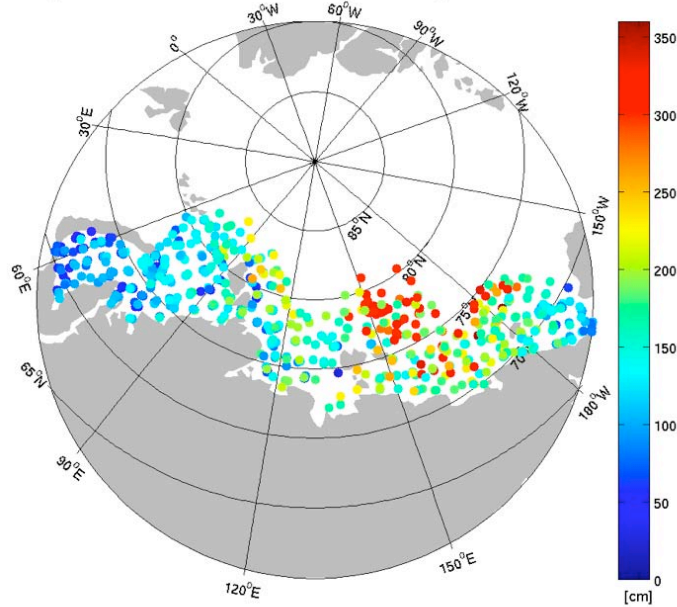
Measurements were made using yardstick in drilled holes on runways (Fig. 1.3), where the airplane landed, and on surrounding ice. Their accuracy amounts to 0.01 m. The data were during the 1980s mostly obtained on first-year ice in the Eurasian Russian Arctic (Figs 1.1 and 1.3).

Runway ice thickness from Russian aircraft landing observations in the 80s



a

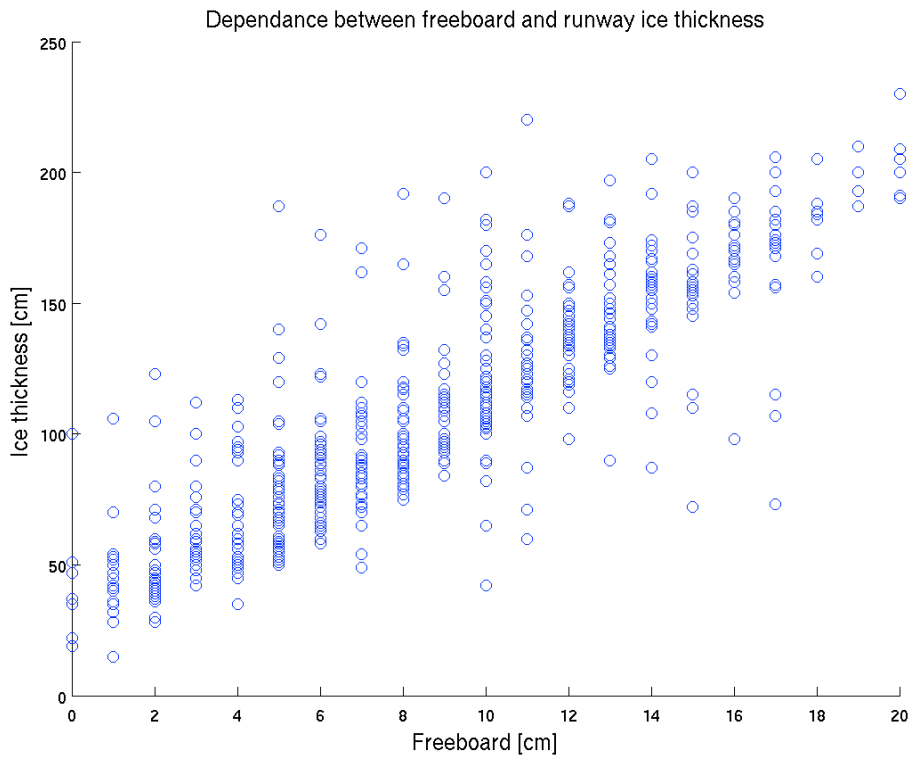
Prevailing ice thickness from Russian aircraft landing observations in the 80s



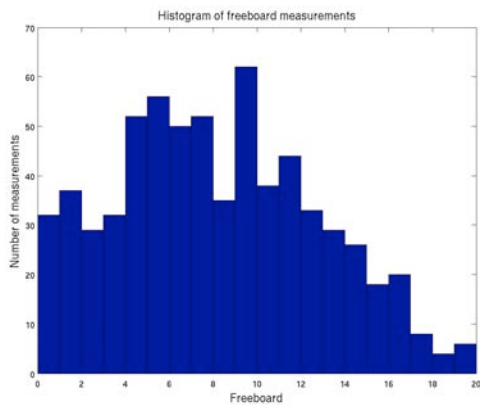
b

Figure 1.3 (a) Ice thickness measurements on both runway and surrounding ice; (b) ice thickness data on runway only.

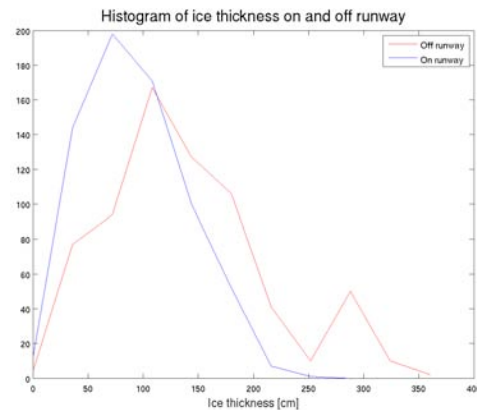
The freeboard was measured on runways with relatively level ice, where thickness could reach up to 2.6 m. The scatter plot of ice thickness versus freeboard measurements on runways, conducted is shown in Figure 1.4a. More than 95% of the freeboard values were less than 0.20 m (Fig. 1.4b). Comparison of the ice thicknesses data off runway compared with those on the runways is shown in Figure 1.4c, indicating the off-runway thickness is generally larger since these data include ridges.



a)



b)



c)

Figure 1.4. a) Ice thickness versus freeboard observed during the Sever expeditions in the 1980s; b) Histogram of ice freeboard measurements; c) comparison of ice thickness on and off the runway.

A linear regression equation between average ice thickness and freeboard, derived from Fig. 1.4a is given by

$$H_i = 8.13F_i + 0.37, (R^2=0.996) \quad (1)$$

It can be used for calculation of first-year ice thickness from freeboard values in the range of 0.01-0.20 m, measured in March-May. Appreciable departures of measurements from this dependence can be explained by stochastic variations, as well as regional and interannual changes of ice density and snow loading. Lack of ice thickness/freeboard measurements in other Arctic regions, on thick multiyear ice, as well as in the period October-February, necessitates development of ice thickness calculation technique using the isostatic equilibrium equation.

In this study snow depth was extracted and histogram of the data are presented in Figure 1.5. The median snow depth on first-year ice and its uncertainty amount to 0.05 m and 0.05 m, respectively. Snow depth off runways exceed this value, as evident from their histograms

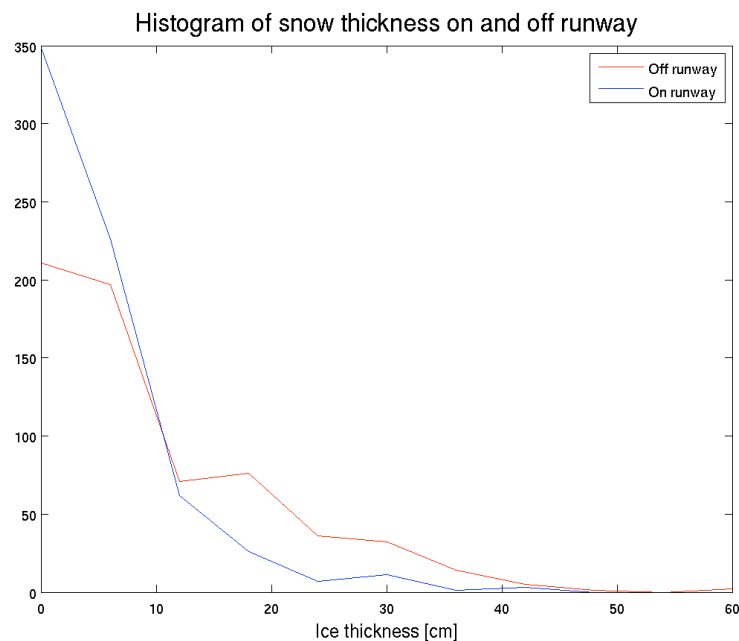


Figure 1.5. A histogram of snow depth values, measured on runways during landings on ice.

In addition to the Sever data, literature studies have been done to find estimates of ice and snow density. The results show that there is significant variability in ice density as reported in the literature (Fig. 1.6), and this is one of the main factors leading to uncertainty in the retrieval of ice thickness from freeboard data.

Average snow depth, snow density, and density of first-year ice from the Sever data, were used in the isostatic equilibrium equation to derive the relation between ice thickness and freeboard for first-year ice (Table 1.3). The multiyear ice in the Arctic has generally lower density and thicker snow cover as compared with the first-year ice. The relation between the thickness and freeboard of the multiyear ice was derived from the isostatic equilibrium equation by using climatological data on snow depth and density and bulk density of ice. The monthly mean snow depth and snow density data are shown in Fig. 1.7.

Table 1.3. Typical values and uncertainties of snow and ice density and snow depth for late winter conditions. The freeboard data are prescribed input to the hydrostatic equilibrium equation.

Parameter	Ice type			
	FY ice		MY ice	
	Typical value	Uncertainty	Typical value	Uncertainty
Ice freeboard, m	0.01-0.2*	0.03-0.08**	0.3	0.03-0.08**
Snow depth, m	0.05	0.05	0.35	0.06
Ice density, kgm ⁻³	916.7***	35.7***	882****	23****
Snow density, kgm ⁻³	324	50	320	20

* the freeboard varies with thickness and age of the FY ice

** freeboard is a free variable and the uncertainty estimates are used as example of realistic numbers

*** analysis of level FY ice from the Sever data

**** based on data from literature

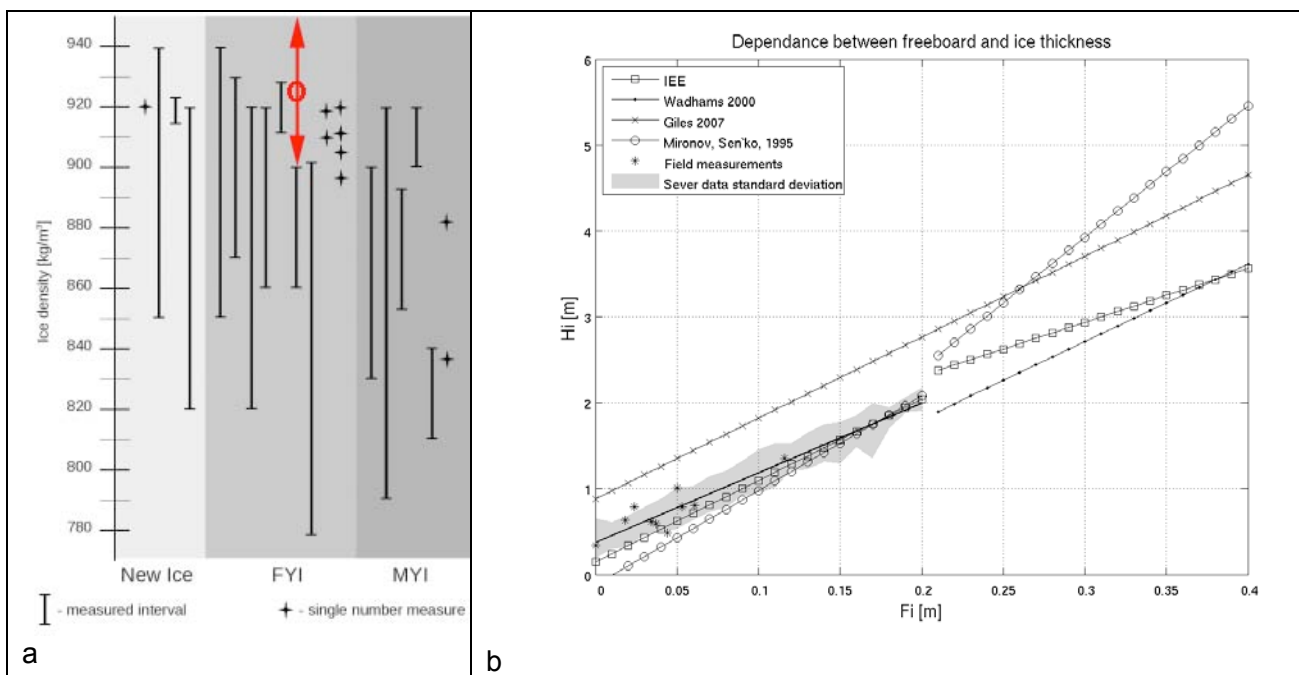


Figure 1.6. (a) Variability of ice density obtained from literature (black lines and crosses) and from analysis of the Sever data (red arrow); (b) relation between ice freeboard and ice thickness based on several data sets and published papers. The Sever data are shown by the bold line with the gray envelope.

The results of the Sever data analysis have been published in the paper “The relation between sea ice thickness and freeboard in the Arctic” (Alexandrov et al., 2010). The paper has analyzed the accuracy of the ice thickness retrieval from freeboard data using documented variability in ice and snow parameters and assumed errors in ice freeboard measurements. The results are presented in Fig. 1.8. For FY ice, retrieval of ≈ 1.0 m (2.0m) thickness has an uncertainty of 50% (40%). For MY ice the main uncertainty is ice density error, since the freeboard error is relatively smaller than for FY ice. Retrieval of 2.3 m (3.0 m) thick MY ice has an error of 20 % (18 %). The

freeboard error used in the calculation is ± 0.05 m for both the FY and MY ice. If the freeboard error can be reduced to 0.01 m, by averaging a large number of measurements from CryoSat, the error in thickness retrieval is reduced to about 32 % for a 1.0 m thick FY floe and to about 16 % for a 2.3 m thick MY floe. The remaining error is dominated by uncertainty in ice density.

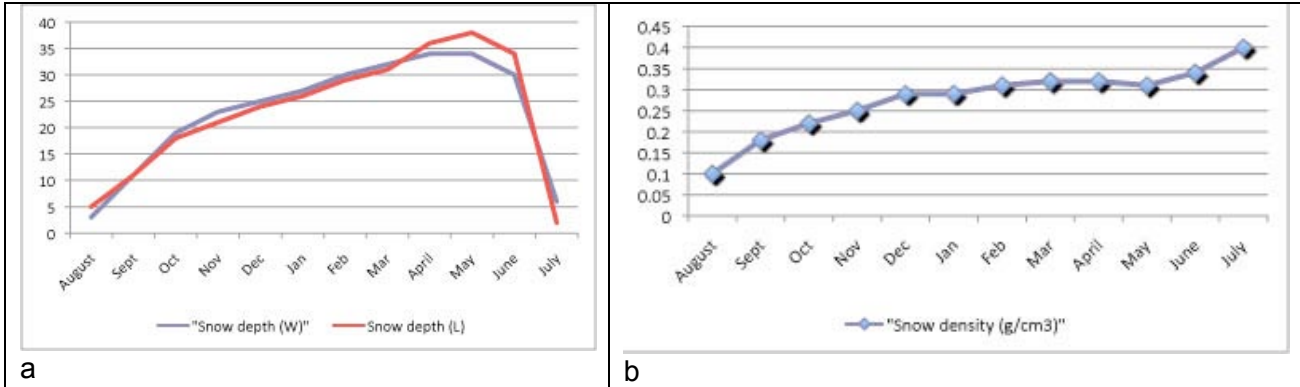


Figure 1.7. (a) Monthly mean snow depth in the Arctic from two sources Warren et al., 1999, and Loschilov (1964); (b) monthly snow density data.

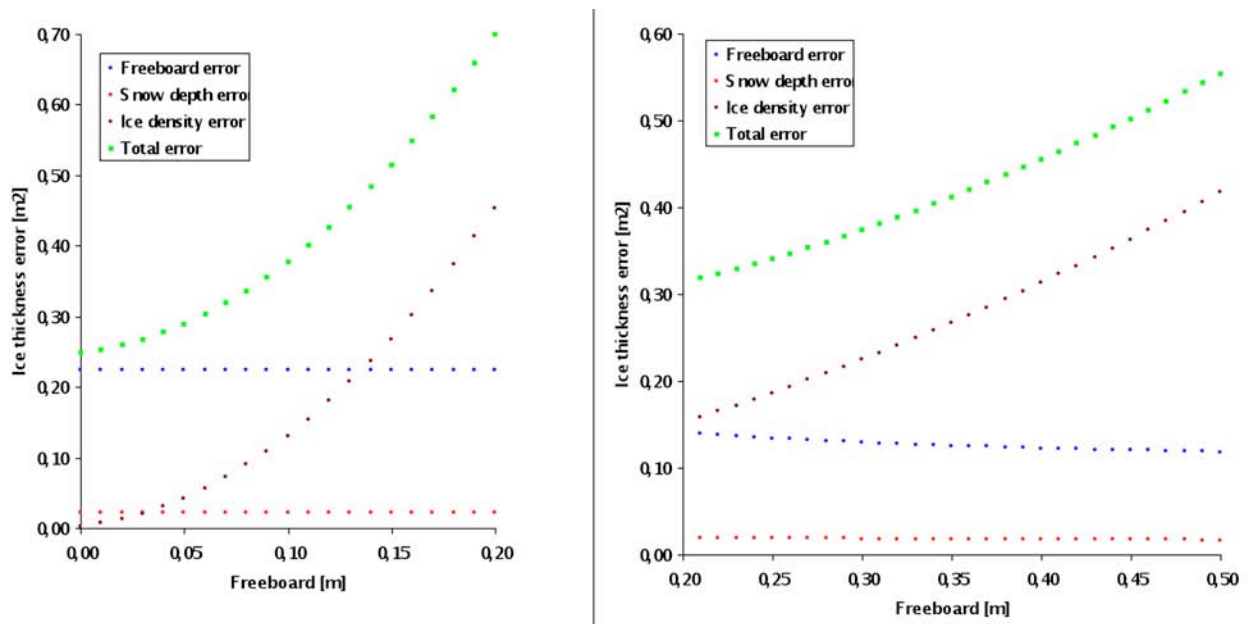


Figure 1.8 Error terms contributing to uncertainty in ice thickness retrieval from freeboard measurements for first-year (left) and multiyear (right) ice. The prescribed error of ice freeboard is 0.05 m.

Two major factors that have implication for ice thickness retrievals from CryoSat are: 1) the error in freeboard estimation and 2) the ice density value used in the isostatic equilibrium equation. Snow depth is also important, and it is necessary to improve the climatological data which are different for MY and FY ice. When averaging freeboard measurements by CryoSat over an area, the error is reduced by a factor $n^{0.5}$, where n is the number of averaged data points. In an area of for example 50 km by 50 km centred at 80°N, about 10 tracks from CryoSat will cover the area from ascending and descending orbits, respectively. With 250 m spacing between each data

point, there will be about 400 data points in one month in the area. Furthermore, if 90 % of the data are diffuse echoes from ice floes and 10 % are specular echoes from thin ice in leads, there will be 40 data points from which the freeboard can be calculated. Assuming that the error of a single measurement is 30 cm, the average freeboard error will be about 5 cm. According to the estimates above, MY ice of 2.3 m thickness will have an error of ± 20 % due to freeboard measurement error.

The choice of ice density in retrieval of ice thickness from freeboard data has strong impact on the calculated ice thickness. As an example, a freeboard measurement of 30 cm will result in ice thickness of 3.5 m if a density of 910 kgm^{-3} is used and 2.2 m if a density of 840 kgm^{-3} is used. Both ice densities are well within reported values from various studies of MY sea ice density. Also FY ice has density within the range $840 - 910 \text{ kgm}^{-3}$ but most observations are in the upper part of the interval, resulting in a higher mean density for FY ice compared to MY ice.

WP2: Report on radar and laser data from airborne campaigns

WP2: Analysis of radar and laser data from previous and new airborne campaigns, including validation data from in situ measurements.

Several CryoSat pre-launch campaigns have been conducted in the spring seasons in recent years over sea ice and icecaps, using the airborne radar instruments ASIRAS and D2P (Delay-Doppler Phase Monopulse radar), together with scanning laser and nadir video. Measurement lines have been flown over sea ice at various altitudes, in order to simulate the Cryosat-2 SIRAL instrument vertical ("normal") incidence measurements. Data available for comparison with SIRAL include airborne EM ice thickness measurements (Haas et al., 1997, 2008), in situ data and satellite SAR and optical images.

The first airborne campaigns with D2P radar in the Fram Strait (near 82N, 10E) took place in 2002 – 2003 with a US-aircraft (Leuschen and Raney, 2006), coordinated with the ship Polarstern and overflights with a Danish aircraft with laser altimeter. A report on these campaigns has been provided by Sandven et al., (2005).

The airborne campaign in 2006

ASIRAS is an airborne version of SIRAL (Synthetic Aperture Interferometric Radar Altimeter flown on Cryosat-2). It has been used in several airborne campaigns together with laser scanner. A detailed report of the CryoVEx 2006 experiment is provided by Stenseng et al., (2007). This report describes the airborne part of the experiment and the processing of the collected dataset. The airborne part of the campaign was carried out by the Danish National Space Center (DNSC) using a Twin-Otter chartered from Air Greenland. The main purpose was to collect coincident ASIRAS and laser data at validation sites placed on land ice and sea ice in the Arctic area and offer logistic support to ground teams. The data collected will be important for the understanding of CryoSat-2 radar signals. A number of overflights of corner reflectors both on sea ice and inland ice will support the studies and calibration of ASIRAS data. The airborne part of the CryoVEx 2006 campaign has successfully been carried out by DNSC during the period April 18 to May 18. A collaboration between ESA, AWI and DNSC has ensured a solid processing of data where many minor and major problems have been identified and solved. A description of the airborne system, the campaign, and the processing is given together with a short description of each validation site. This should aid the user in the understanding and correct use of the dataset.

In addition to the airborne campaign carried out by DNSC, several independent in-situ data on ice thickness and snow depth were collected during CryoVEx 2006 on two large ice floes north of Alert; additional scientific activities included flights with the AWI EM-system, which provides an independent estimate of sea ice thickness. A report on the in situ measurements performed from Alert/Northern Ellesmere Island is provided by Haas et al., (2006).

The ASIRAS system was built by Radar Systemtechnik (RST) of Switzerland with support of AWI and Optimare. It operates at 13.5GHz with bandwidth of 1GHz, beam-angle 10° along-track and 2.5° cross-track (footprint 50m x 5m at 1100m height). Further description of the ASIRAS 2006 data is provided by Stenseng et al., (2007) and Cullen (2007).

In this study, a set of ASIRAS data taken over sea ice and available by ftp from an ESA server, have been downloaded and processed. Data are selected from a section in northern Fram Strait on 02 May 2006 during the transit flight from Longyearbyen to Station Nord. A map of the CryoVEx 2006 flights is shown in Fig. 2.1.

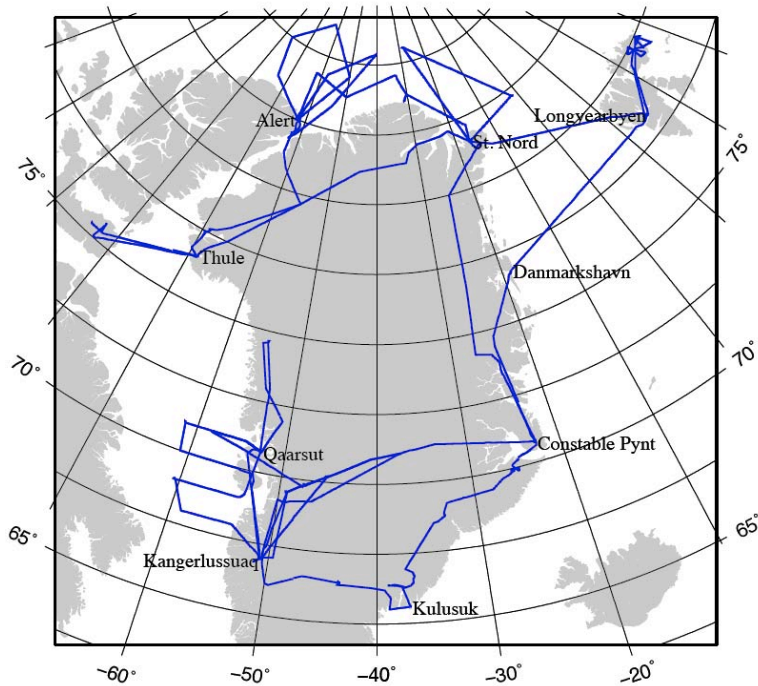


Figure 2.1: Tracks flown during CryoVEx 2006 by the Air Greenland Twin Otter equipped with the DNSC laser scanner system and the ASIRAS radar (Stenseng et al., 2007).

The ASIRAS data from the Fram Strait overflight have been processed to profiles with signal strength and height as function of time. These have been co-located and compared with ASAR Wideswath images available as close to the flight times as possible. Correction of the ice drift during these time differences between data has been estimated by using another ASAR scene of the ice on the same day.

ASIRAS data from 02 May 2006

The comparison for 2006 has been made with 4 flightline sections: A01 – A04 obtained on 02 May between 10z and 11z as shown in Table 2.1.

Table 2.1. ASIRAS data sets from the Fram Strait flight lines on 02 May 2006

Profile	Start	Stop	Duration	File size	rec"s	lines	Dataset
A01	10:16.4	10:24.6	8.2 min	30Mb	171	3420	AS01
A02	10:25.8	10:31.3	5.5 "	54 "	306	6120	AS02
A03	10:34.0	10:39.6	5.6 "	18 "	100	2000	AS03
A04	10:40.2	11:01.5	21.3 "	205 "	1150	23160	AS04

The ASAR image of 02 May 2006 12:50z and ASIRAS profiles are shown in Fig. 2.2. The ice edge is to the right with windy water outside (bright). Large floes are grey (wet snow), larger leads /polynyas are dark (smooth ice /calm water). The flight line crossed the ice edge in the northern part of the Fram Strait during transit from Longyearbyen to Station Nord was selected since an ASAR Wideswath image for this area was available on the same date at 12:50z. The ice edge crossing at about 10:15z was just off the eastern edge of the image (Fig. 2.2). The fastice flaw zone off the coast of Greenland was crossed at about 11:15z. Accurate registration of the ASIRAS profile with the ASAR pixel values has been made. The time difference between the two datasets is about 2 hours, the pack ice motion is estimated to be about 1km, which is roughly the accuracy of geolocation of the ASAR image.

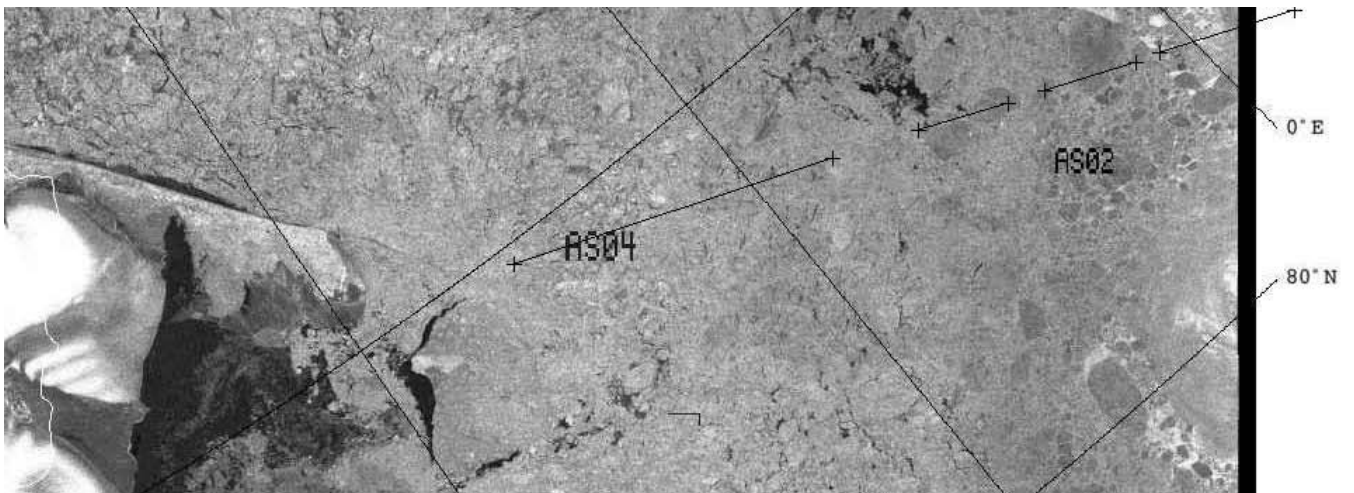
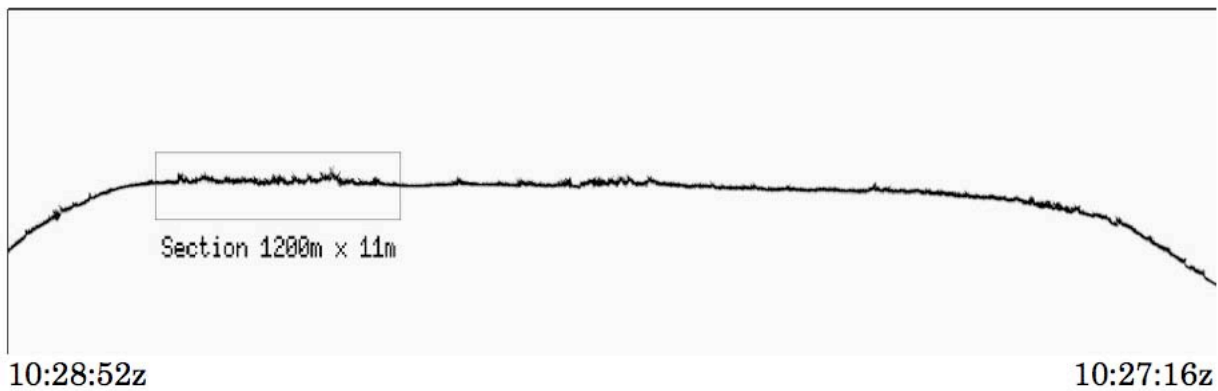
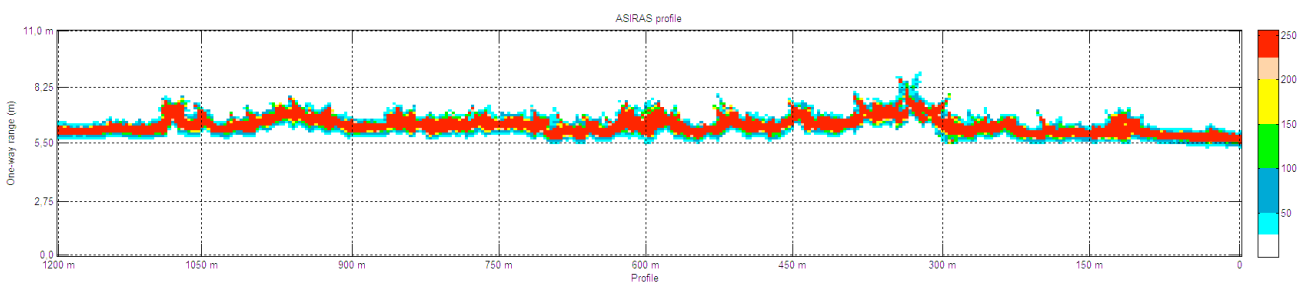


Figure 2.2. Subset of ASAR Wideswath image 02 May 2006 12:50z with the 4 ASIRAS flight-line sections A01 (crossing the border at upper right near the ice edge) to A04 (in the middle of the image near the NE-Greenland coast). Lines A02 and A03 cross over large ice floes with low backscatter.



a



b

Figure 2.3. The ASIRAS height signal as function of flight distance for profile line AS02 (crossing a large ice floe). The length of the section shown is 5.6 km. (b) A sub-section of 1.2 km length shows the pulse reflected from the ice surface in full resolution. The peak of the signal, which is marked in red, represents the multi-look power echo normalized to 255. The signal resolution (sampling) is 0.11 m in height and 3.4 m in horizontal distance. Variations in freeboard height up to about 0.4m can be seen over distances of the order of 30 - 50m. Processing of the ASIRAS data is described in Appendix A1. Calculation of height range is described in the example from 02 May 2008.

Data from a subset of the A02 flight-line is presented in Fig. 2.3. The red colour in the ASIRAS signal, corresponding to the peak of the signal, has a width corresponding to a height difference of approximately 0.3m. Variation in freeboard height up to about 0.4 m can be seen over distances of the order of 30 -50m.

The airborne campaign in 2008

The airborne part of the CryoVex 2008 campaign was carried out by DTU Space (former Danish National Space Center, DNSC) using a Twin Otter chartered from Air Greenland. The main purpose was to collect coincident ASIRAS and laser elevation data from validation sites on land and sea ice and in addition offer logistical support to ground teams. Overflights of corner reflectors were done at main validation sites in order to calibrate the ASIRAS data. The airborne part of CryoVEx 2008 was successfully carried out between April 15 and May 8. The airborne system, the field work, and the data processing together with short descriptions of each validation site are presented in detail in a report by Hvidegaard et al. (2009). The data from AWI's helicopter electromagnetic sea ice sounder (EM bird) along with the field report of the sea ice in situ validation work carried out near Alert in May 2008 is provided by Haas et al. (2008).

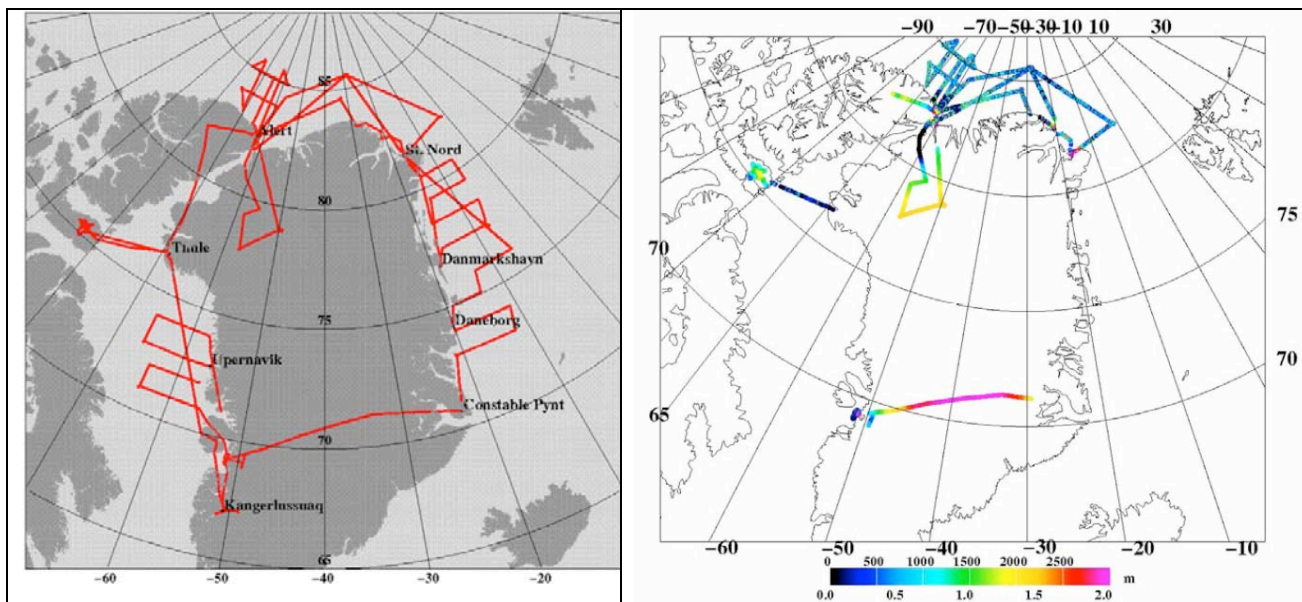


Figure 2.4. The left map shows an overview of the CryoVex 2008 flights from 15 April to 08 May. The right map show the flight tracks where laser scanner data were obtained. The colour codes for the sea ice areas show the heights relative to local sea level (Hvidegaard et al., 2008).

ASIRAS 24 April 2008

On 24 April 2008 several flight line sections were obtained over the sea ice in the Fram Strait. A MODIS image with flightline overlays between 77° and 80° 30'N is presented in Fig. 2.5a. The flight line A06, which is selected for presentation of ASIRAS data, covers the southern part of the Fram Strait, approximately 100km in from the ice edge, in the area where RV Lance was located. Several short flights were obtained over the Lance area. The A06 flightline is also shown in a zoomed image, where also the ASIRAS data are shown for a 3.6 km long section (Fig. 2.5b). The MODIS image does now show any details of the ice along the flightline, except for a lead in the northern end of the line.

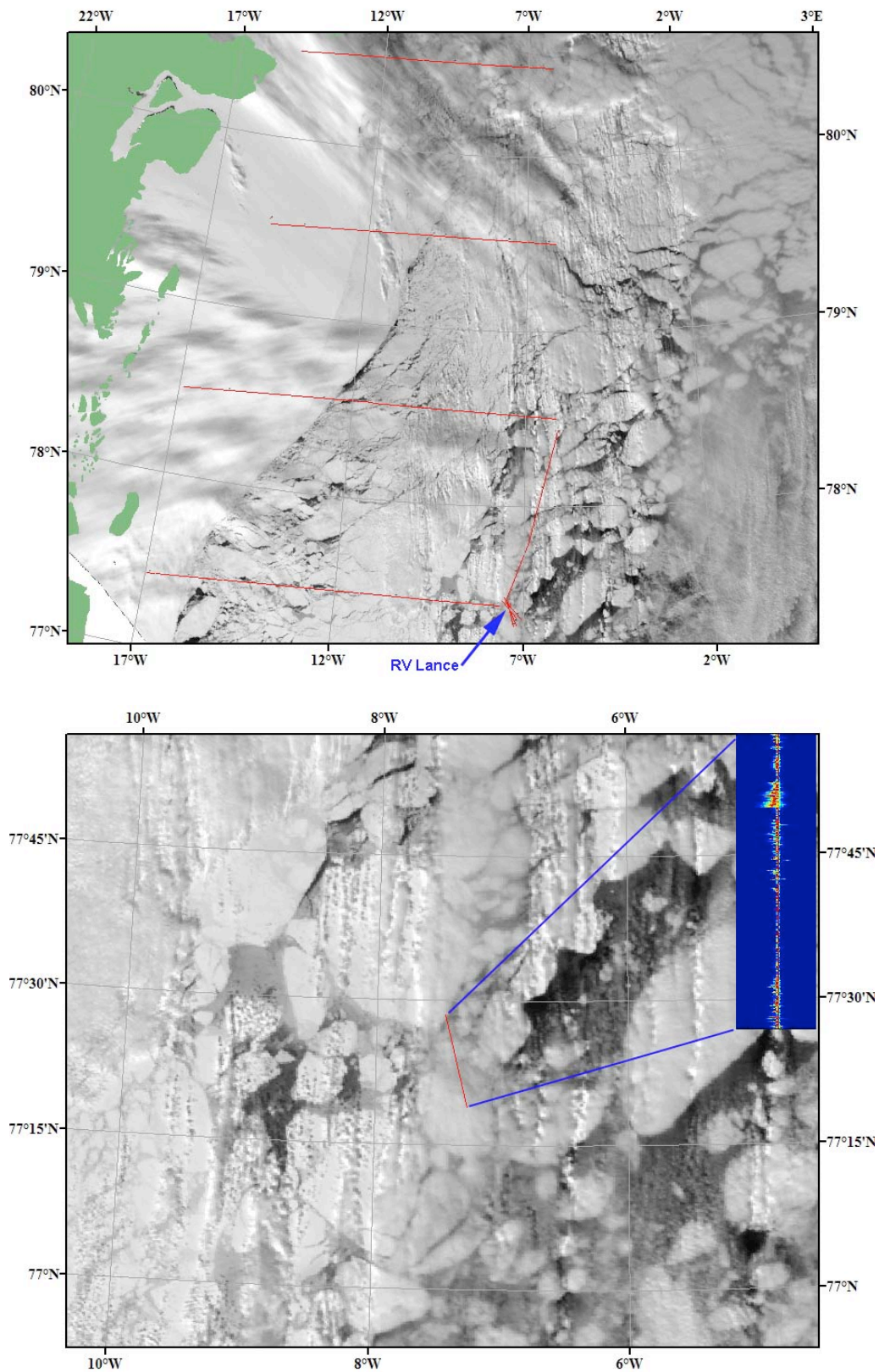
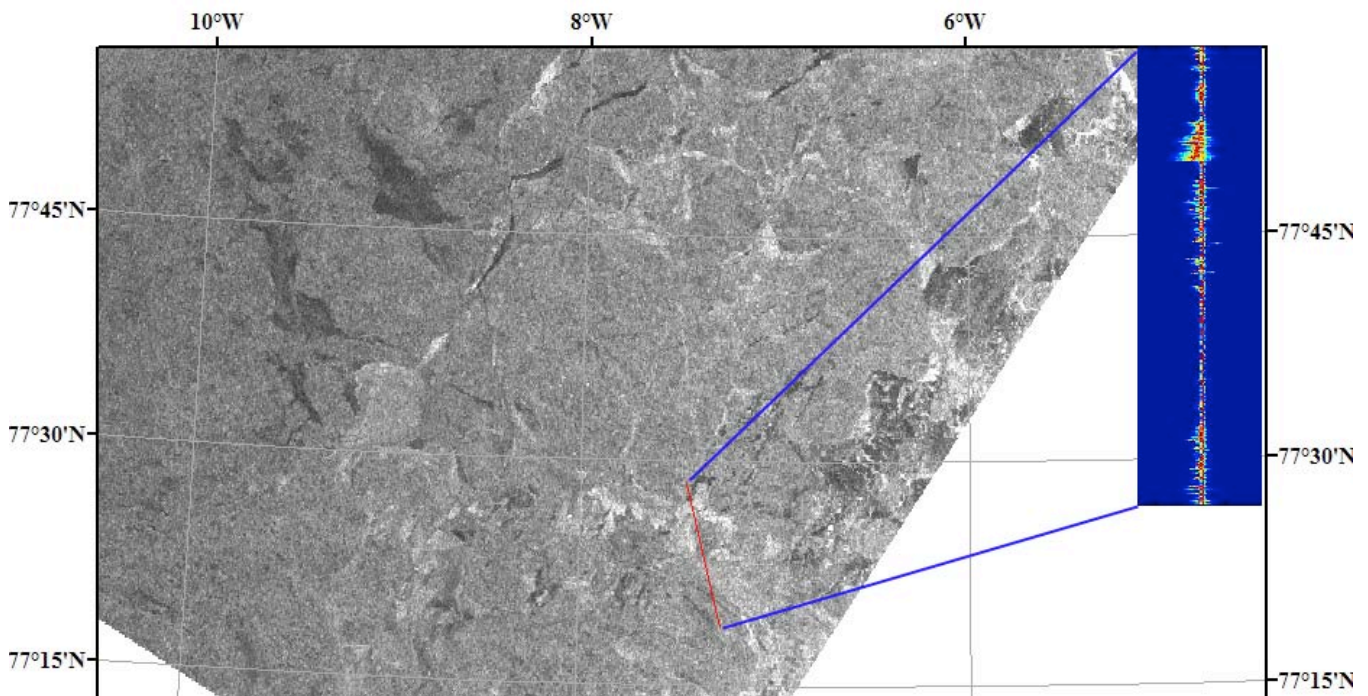
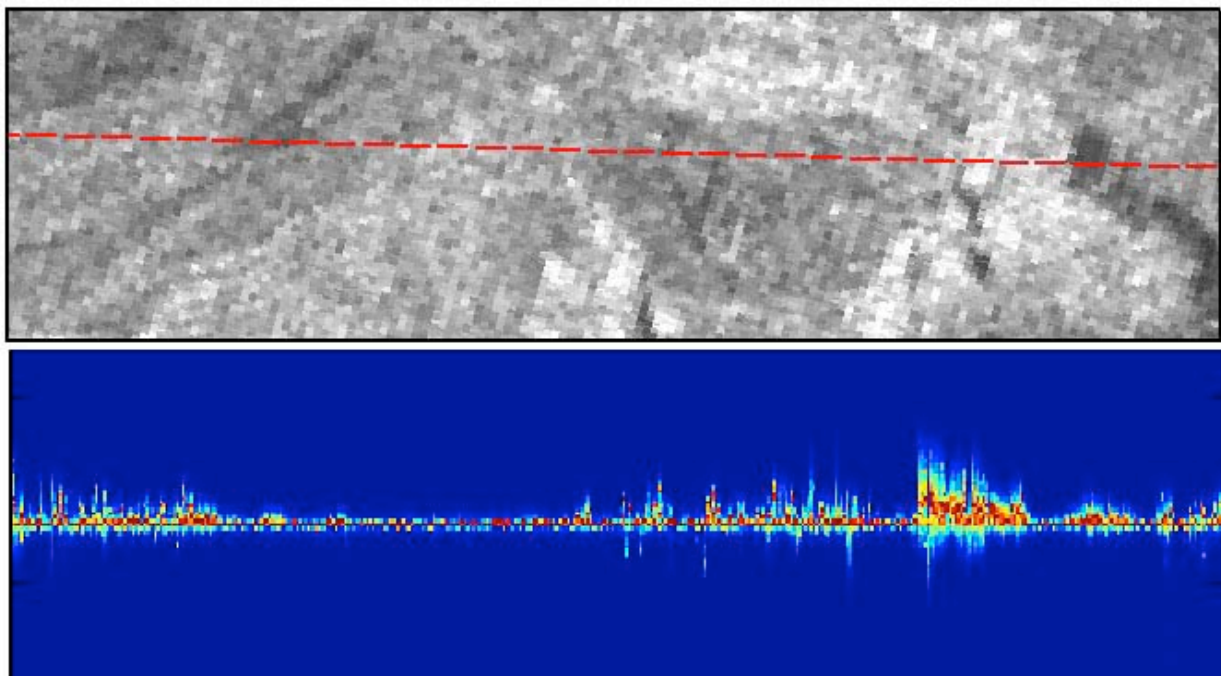


Figure 2.5. The upper map is a MODIS image form the Fram Strait on 24 April 2008, with flightlines showing where ASIRAS data were obtained. The lower figure is a subset of the MODIS image with flightline A06 marked in red and the ASIRAS data in the upper right corner.

The flightline covers ice with variable backscatter in the SAR image, as shown in Fig. 2.6. where the ASIRAS and SAR data are collocated. Laser data and nadir photographs are not available for this flightline.



a



b

Figure 2.6 (a) SAR image with flightline A06 overlaid (redline) and the ASIRAS data in the upper right corner. (b) collocated ASAR and ASIRAS data.

ASIRAS 02 May 2008

On 02 May ASIRAS data were obtained in the Lincoln Sea north of Ellesmere Island /Station Alert, along meridian 65.17W. A SAR WSM image from ENVISAT over this area was available on the same date, when also helicopter surveys with EM sensor were obtained along the same line as the ASIRAS flights (Fig. 2.7a). The ice thickness data from the EM survey are superimposed on the SAR image, showing that the large lead with refrozen firstyear ice has thickness less than 2.0 m, while the multiyear ice north of the polynya has thickness above 3 m. Sub-images the SAR and MODIS image covering the transition zone between the refrozen polynya and the multiyear ice is shown in Fig. 2.7 b and c..

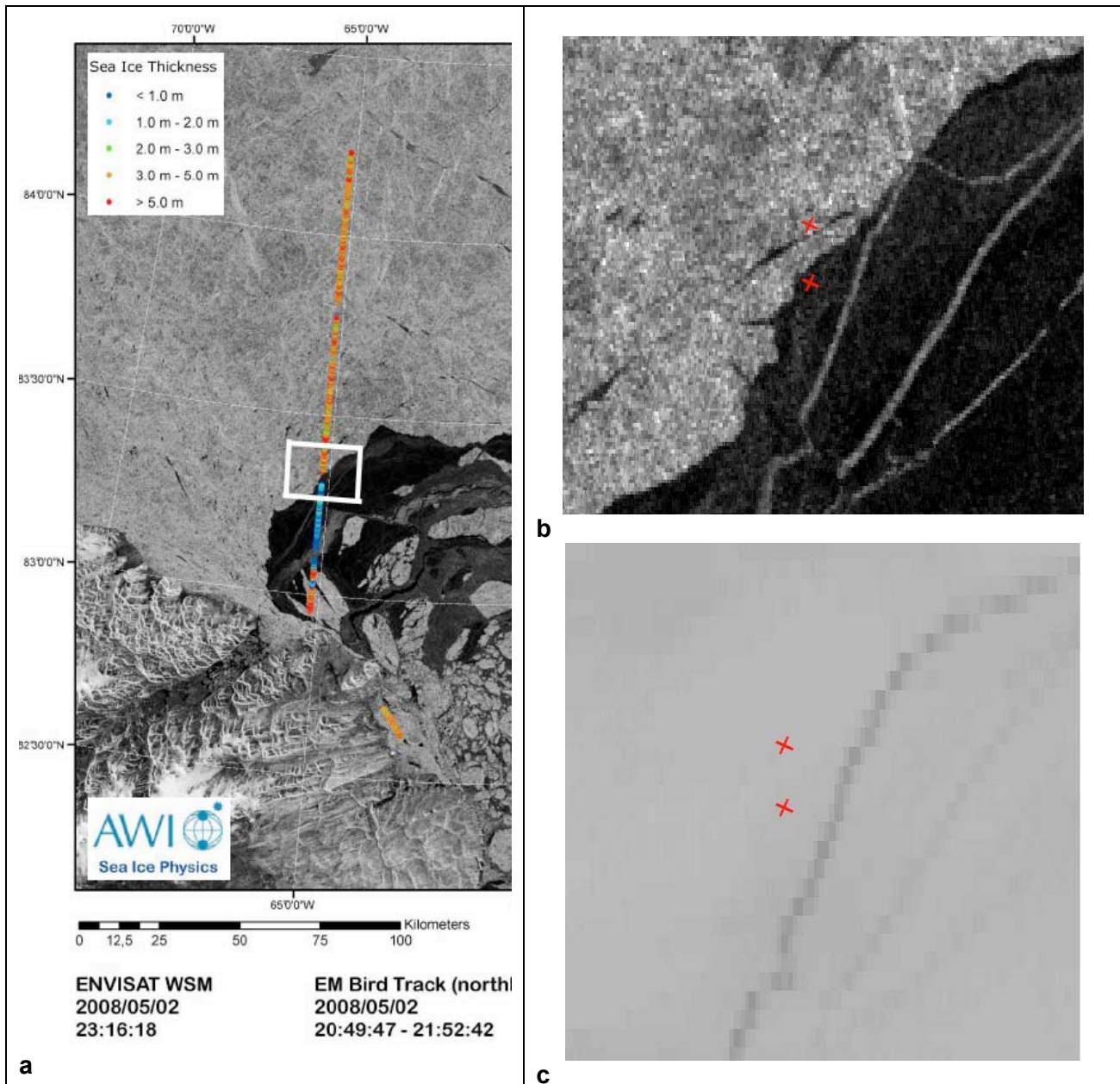


Figure 2.7. (a) Part of an ASAR Wideswath image obtained north of Ellesmere Island on 02 May 2008 with EM thickness data superimposed; (b) Subset of the SAR image, located in the white box in (a); (c) subset of a MODIS image on the same day. The red crosses mark a sub-set of the flight line where ASIRAS data, ALS (AWI Laser Scanner) data.

The ASIRAS data from 02 May covers multiyear ice north of Ellesmere Island with fairly uniform backscatter, without any clear leads or other ice features along the flight-line. In the following figures, examples of ASIRAS, ALS and nadir-looking photographs are presented and discussed. The examples are taken from the transition zone between the polynya and the multiyear ice. Comparison of collocated ASIRAS and ALS data is shown in Fig. 2.8 and Fig. 2.9.

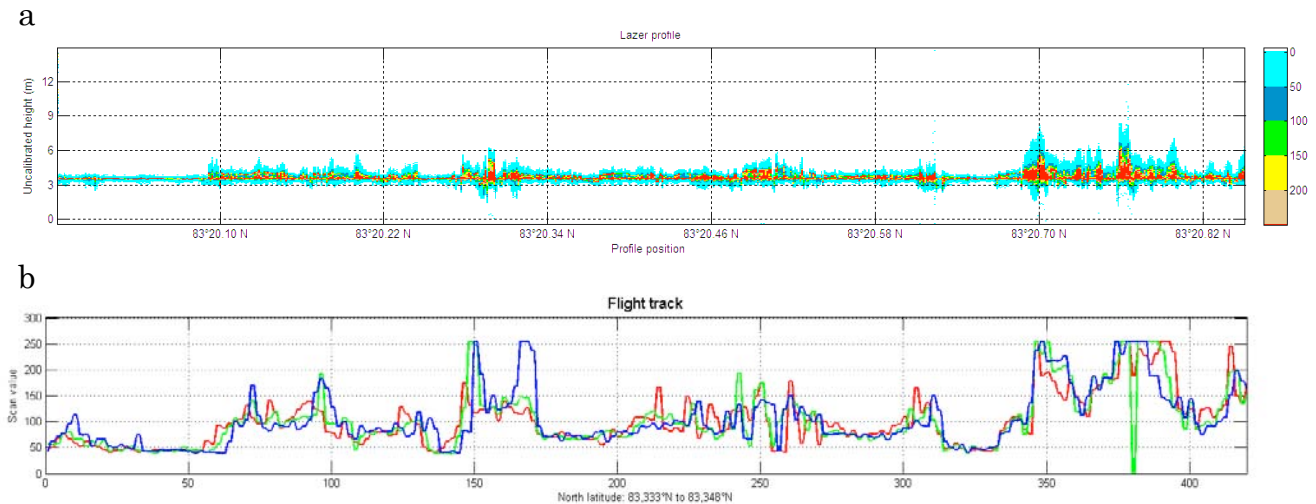


Figure 2.8. (a) A sub-section of the ASIRAS data of length 1150 m obtained around 21:25:40z, located at the transition between level firstyear and deformed multiyear ice. The resolution is 2.3m in horizontal distance and 0.11m in height. The maximum values corresponding to multi-look power value above 5000 has a width of 0.2 -0.3 m. Many sharp peaks of height 1.0 – 1.5 m and also noise above the main signal are observed. (b) Laser profiles (3 parallel lines in the centre of the scanning laser image) co-located with the ASIRAS data. Processing details for ALS data are given in Appendix.

Calculation of height range in ASIRAS data

For LAM_A data with 1024 samples, equation 3.2-6 in the Product Description (Cullen 2010), gives the following formula for the measured range (height):

$$R = (c * T_{uc} / 2B) * (F_{off} + F_s * (n - N/2) / N)$$

Where

$c = 299792458$ m/s = speed of light,
 $T_{uc} = 80$ microsec =uncompressed pulse length,
 $B = 1$ GHz = bandwidth,
 F_{off} = initial LAM offset.freq. obtained from ASIRAS log file,
 $F_s = 9.375$ MHz = instrument sampling frequency,
 $N = 1024$ = number of echo samples (bins)
 n =signal bin number (1 to 1024).

The range for a LAM_A signal at the center bin number 512, assuming $F_{off} = 60$ MHz is: $12 * 60 = 720$ m. This will be the nominal flight altitude. The sensitivity (range per bin no.) is: $12 / 1024 = 0.117$ m

However, the processed data are of type ASI_W, that is “windowed” and with 256 bins. Assuming a sensitivity equal to LAM_A, the height of the box in Fig. 2.8a (“range” of the profile signal) is

then $256 * 0.117\text{m} = 29.95\text{m}$. Since this is 2-way distance, echo surface-height variations correspond to half this value, that is 15m range of the ice surface.

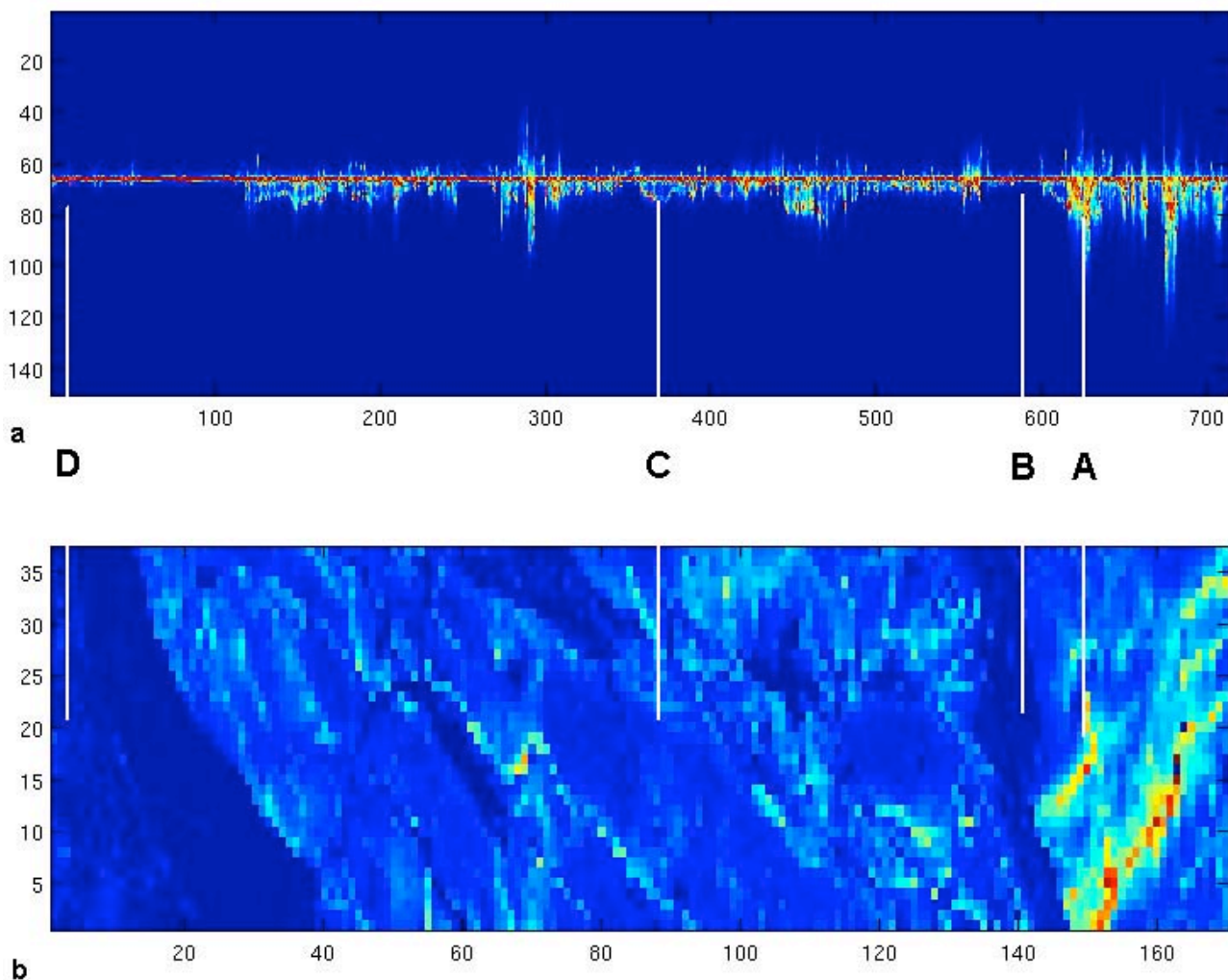


Figure 2.9. (a) ASIRAS waveform data where the vertical axis is uncalibrated values in the range 55 – 120 out of the original 256 bins. Time delay increases downwards. The length of this section of 725 lines is 1620m (2.23 m/line). (b) ALS image showing height above a given reference level (Stenseng et al., 2007, Hvidegaard et al., 2009) where dark blue is level ice and yellow-red are ridges up to 2 m. The width of the ALS image is 240 m and the length is the same as in (a). The horizontal axis represents time and distance as the aircraft travelled from south towards north (the same axis as in Fig 2.8). The vertical white lines show the position of case A, B, C and D where waveform data are plotted (Fig. 2.10).

Figs. 2.8 and 2.9 show ASIRAS and ALS data at the crossing of the FY/MY ice boundary on the northward flight. In ALS data the area of thinner ice to the left has lower height (that is: darker) compared to the thick ice area to the right. In the thick ice area several ridges of various widths and heights are observed, To the right there are ridge above 2 m in height. In the ASIRAS data the level ice has a narrow wave form while the ridged ice has a broader waveform. Narrow waveform indicate a mirror-like signal with a trailing edge that is as steep as the leading edge. Accordingly, little or no echo signal is received from the smooth ice outside of the (near circular) backscattering area situated at the nadir of the instrument. Examples of waveform data are shown in Fig. 2.10.

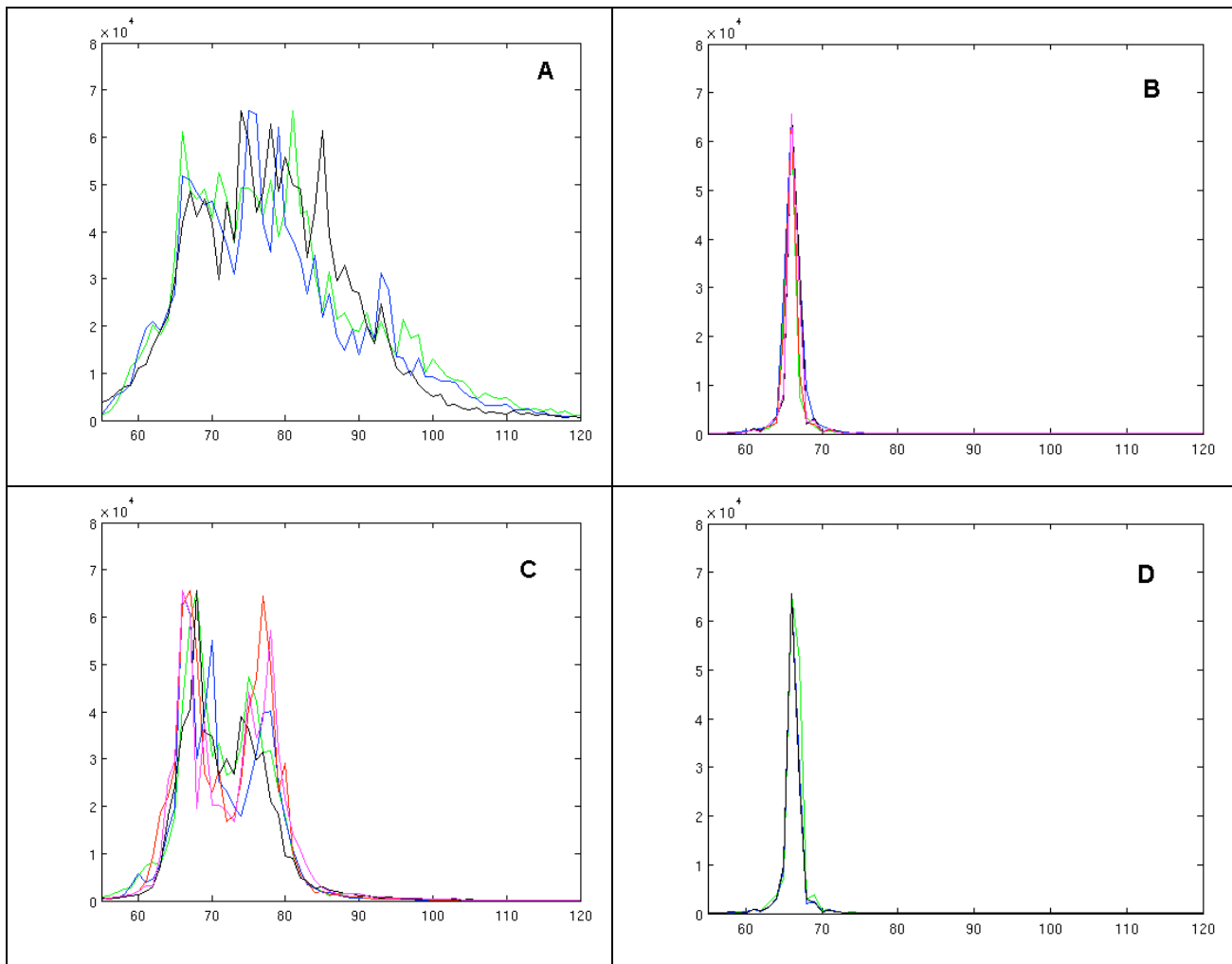


Figure 2.10. Example of wave form data in four different locations, corresponding to A, B, C and D in the timeseries in Fig. 2.9. Each figure shows several adjacent waveforms, presented as uncalibrated values in the range 55 – 120 out of the original 256 bins. Time delay increases with increasing value along the x-axis.

The waveform data in Fig. 2.10 can be described in terms of the specific ice conditions observed by scanning laser data and nadir-looking photographs. Example of co-located laser and photographs are shown in Fig. 2.11. Waveform data in a typical ridge area (photo at 21:16:37) are shown in A. This waveform has a broad peak with long trailing edge. Waveform data from a lead surrounded by ridges is shown in B, with a characteristic narrow peak. The lead is visible in the photos from 21:16:33 and 21:16:37. C shows waveforms from typical rough multiyear ice without any dominating ridges. These waveforms have two peaks and are more narrow than case A. In case D, the waveform from a refrozen lead has a narrow peak similar to case B.

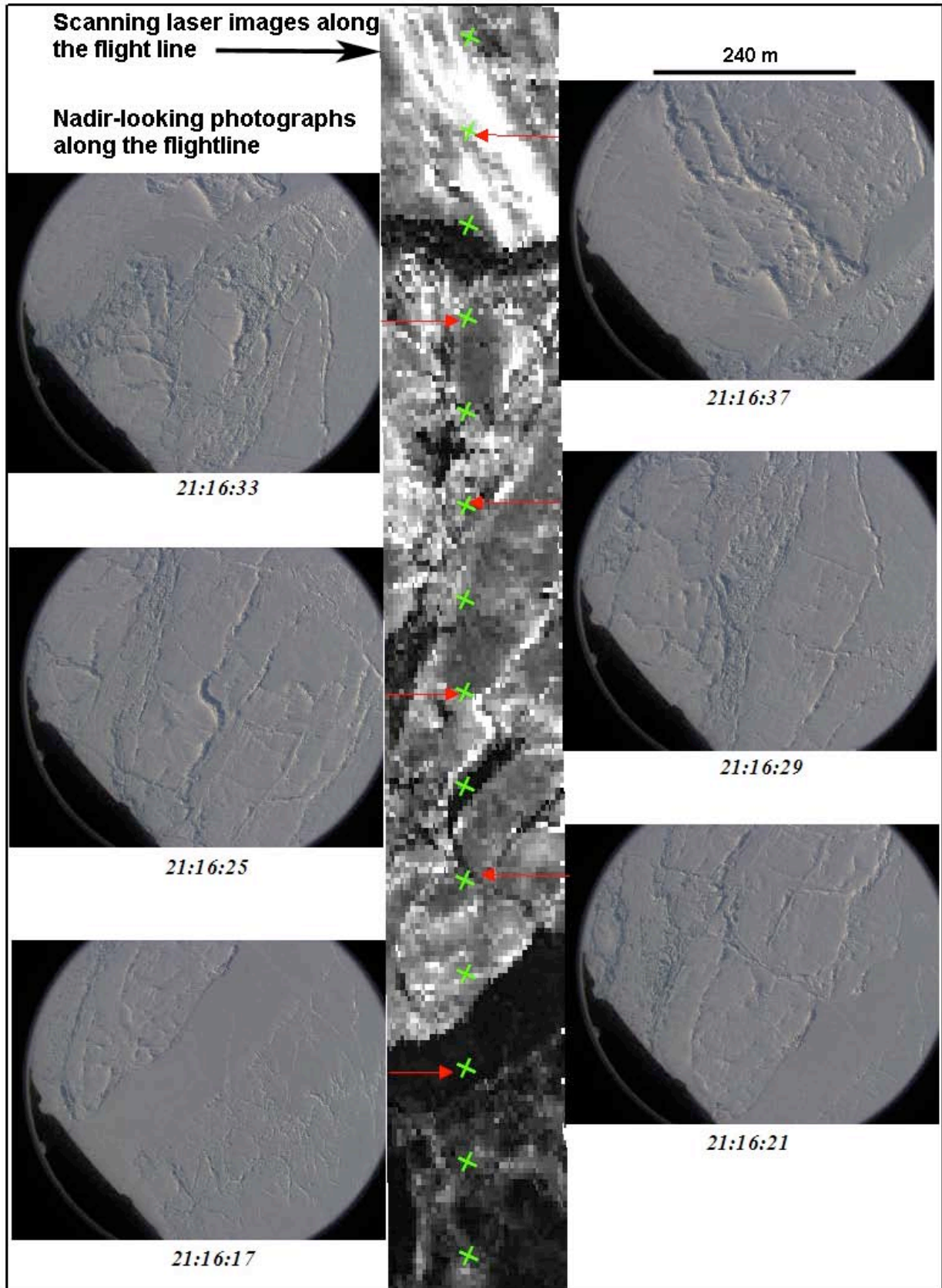


Figure 2.11. Comparison of nadir-looking photographs and scanning laser data along the flight line (shown also in Figs. 2.8, 2.9 and 2.10). The green crosses correspond to the centre point in each image.

Over the rough MY ice the waveform data have a varying slope length of the trailing edge. This is seen as varying broad signals “spikes” upward from the main (profile peak) signal. Accordingly over this ice, a significant echo signal is also received from the rougher ice outside of the nadir area. Due to the SAR processing in azimuth, this echo comes mainly from areas adjacent to nadir in the range direction, perpendicular to the nadir line. The leading edge of the signal profile shows overall little variation in its echo time (height) over the whole profile section processed, with no abrupt change seen at or near the ice boundary. This indicates that the freeboard is fairly constant over the whole section, within about 0.1m.

Some scattered echo signals are seen below the main (profile peak) signal. The strong echoes are probably due to signal from top of ridges. The strong early echoes are most clearly seen over the broad ridges situated to the right in the ALS image. Also, over ridges the trailing edges of waveforms are less steep, indicating rough ice where the height from ALS is greatest. Ridge height can be roughly estimated from ASIRAS to be a maximum of about 0.2m. Also some weaker signals are seen below the main peak, corresponding to early echoes. These are probably due to noise (of unknown origin).

In conclusion, a clear difference is seen in the waveform data between the smooth and thin new ice, and the rough and thick MY ice. This will be the main signature for the SIRAL instrument onboard Cryosat-2 for identifying typical echoes from these two types of ice, and its validity should thus be confirmed in our analysis. But a clear signal of a possible jump in freeboard height due to varying ice thickness cannot be found in the ASIRAS data processed here.

WP3: Report on sea ice data from IPY projects

WP3: Obtain and analyse sea ice data from field investigations funded under several IPY projects (DAMOCLES, BIAC, iAOOS, carried out in 2007 – 2010)

Data collection by UNIS in 2008 – 2009

Collection of in situ ice thickness, freeboard and snow thickness data is performed during the annual UNIS cruise with Lance in April. Also ice and snow density data are collected in these cruises (UNIS, 2008). The in situ data are important for validation of the isostatic equilibrium hypothesis, which is used to retrieve ice thickness from freeboard measurements by radar altimeter on aircraft (ASIRAS) and satellite (CryoSat SIRAL). In this section some examples of in situ data from the Lance cruise in 2008 are presented. A summary of the measurements from three ice stations, denoted Grid 1, 2 and 3, are shown in Table 3.1. Each grid is 10 by 10 meters and contains 9 and 25 measurement holes. There is significant variability within each grid, so the average values are considered to be representative for the floe. When a number of such gridded data are collected over larger areas, the data becomes important for validation of radar altimeter data. An example of an ice station with outline of a grid is shown in Fig. 3.1.

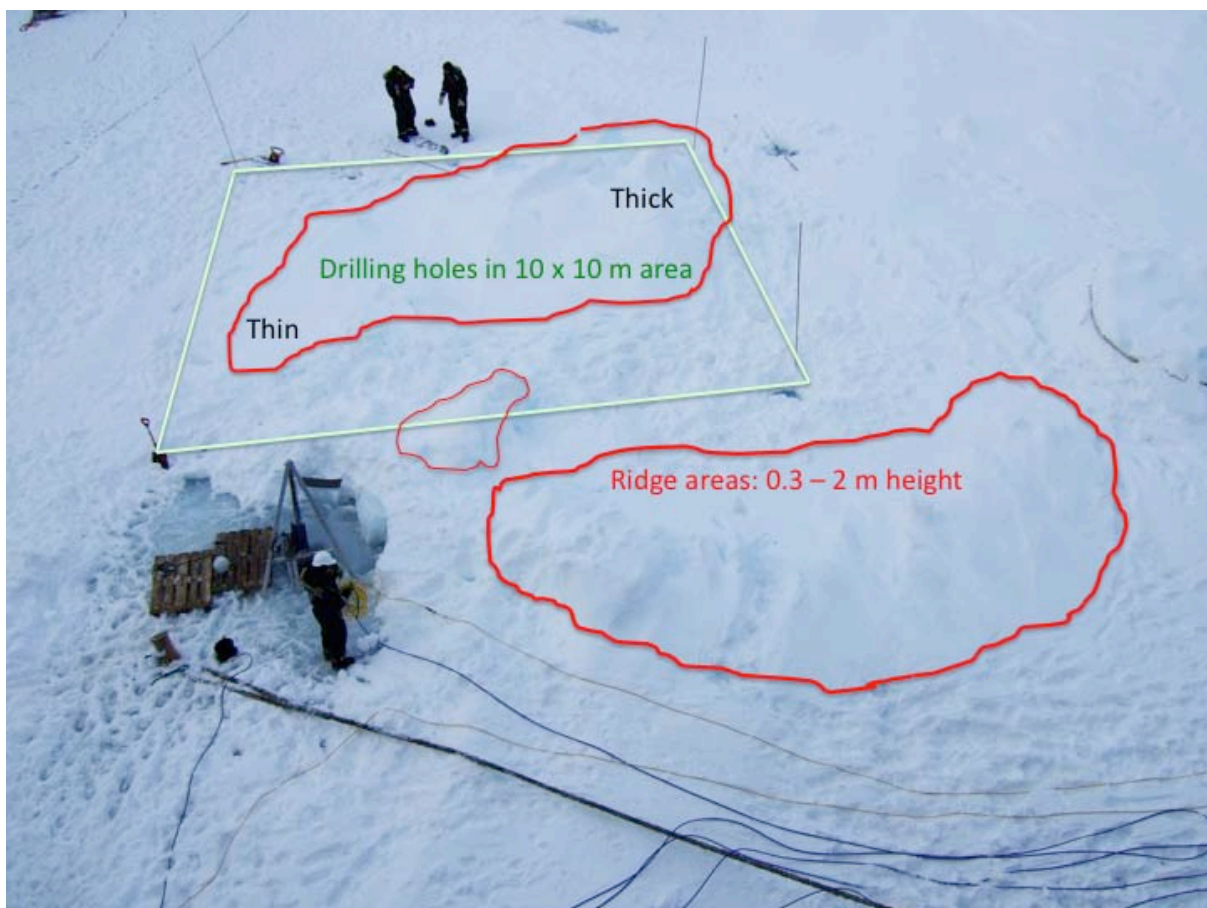


Figure 3.1. The ice station north of Hopen taken in April 2008, where Grid no. 3 is shown by the square. The ice station was taken on a firstyear ice floe with several ridges mixed with level ice. A 3D multibeam sonar (Echoscope™) was deployed through a hole in the ice to measure the topography and draft of the underside of the ridge.

The thickness of the fast ice in Van Mijenfjorden was mapped in two grids by drilling holes and perform direct measurements with a yardstick. Grid 1 was made in an area where the ice was relatively flat, and included nine measurement points with a resolution of 5 m. The standard deviation of the measurements is rather small in this grid, showing that the variability in all four parameters is low. Grid 2 was made in an area where ridging activity had taken place. The standard deviation in all the measured parameters is therefore much larger than in Grid 1. It was assumed that Grid 2 required a higher resolution due to more abrupt changes in the ice thickness, and therefore a grid consisting of five by five measurement points with a resolution of 2.5 m was made. Freeboard was measured in both grids, but snow depth was only measured in the first one, as the snow in the second grid was disturbed by footprints and scooter tracks.

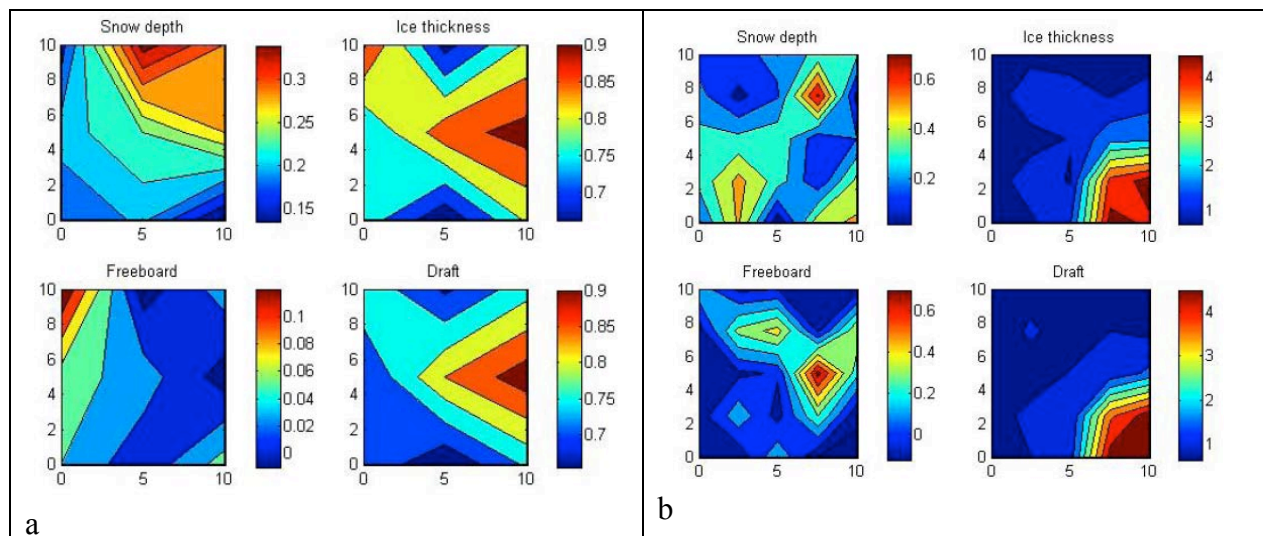


Figure 3.2. In situ data for Grid 1 (a) and Grid 3 (b) where all units are in meter. Note that on local scale ice thickness, freeboard and snow depth can vary strongly.

Table 3.1. Summary of in situ ice and snow measurements from ice stations during the Lance cruise in April 2008.

Ice station	Parameter	Minimum (cm)	Maximum (cm)	Mean (cm)	Standard deviation (cm)
Grid 1 (9 holes) Flat fastice in VanMijenfjorden	Ice thickness	66	92	80	9.4
	Freeboard	-1	12	3.4	4.0
	Draft	65.5	93	76.6	8.5
	Snow depth	13.5	35	23	6.9
Grid 2 (25 holes) Ridged fastice in VanMijenfjorden	Ice thickness	52	201	101.7	41.9
	Freeboard	-16	58	7.2	15.9
	Draft	57	165	94.6	34.2
Grid 3 (25 holes) Deformed firstyear ice North of Hopen	Ice thickness	69	471	158.9	133.7
	Freeboard	-12	74	8.7	21.5
	Draft	64	480	150.2	135.7
	Snow depth	2	72	29.2	17.2

Ice station where ice density was measured	Parameter	Minimum (kg/m ³)	Maximum (kg/m ³)	Mean (kg/m ³)	Standard deviation (kg/m ³)
From 18 cores	Ice density	816	955	902	34

On the drifting ice floe north of Hopen a grid consisting of five by five measurement points with a resolution of 2.5 m was made in Grid 3. The standard deviation of the measurements is significantly higher than for the fastice in Grid 1 and 2. The main purpose of Grid 3 was to map the topography of the underside of an ice ridge in order to validate measurements with a 3D sonar lowered through a hole in the ice (Fig. 3.1). The corners of the grid were therefore chosen such that part of an ice ridge was embedded in the grid. The data for Grid 1 and Grid 3 are presented in Fig. 3.2.

Data collected by UNIS in 2010 using a Geonics EM-31 instrument

During the Lance cruise in April 2010, an electromagnetic sounding system was used to measure ice thickness (Fig. 3.3). There are several different types of EM systems, some are operated from aircrafts or ships, others from the ground (Haas et al., 1997). In this task the EM-31 Ice was used, which is an instrument made for ground based measurements. Studies by Haas et al. (1997) have proven this instrument to be well functioning and able to give highly reliable results over level and moderately deformed ice. On the Lance cruise the ice thickness distribution on fjord ice and at two ice floes was investigated. And on the same time the EM-31 instrument was tested against drillhole measurements to see how to best get reliable results from it.

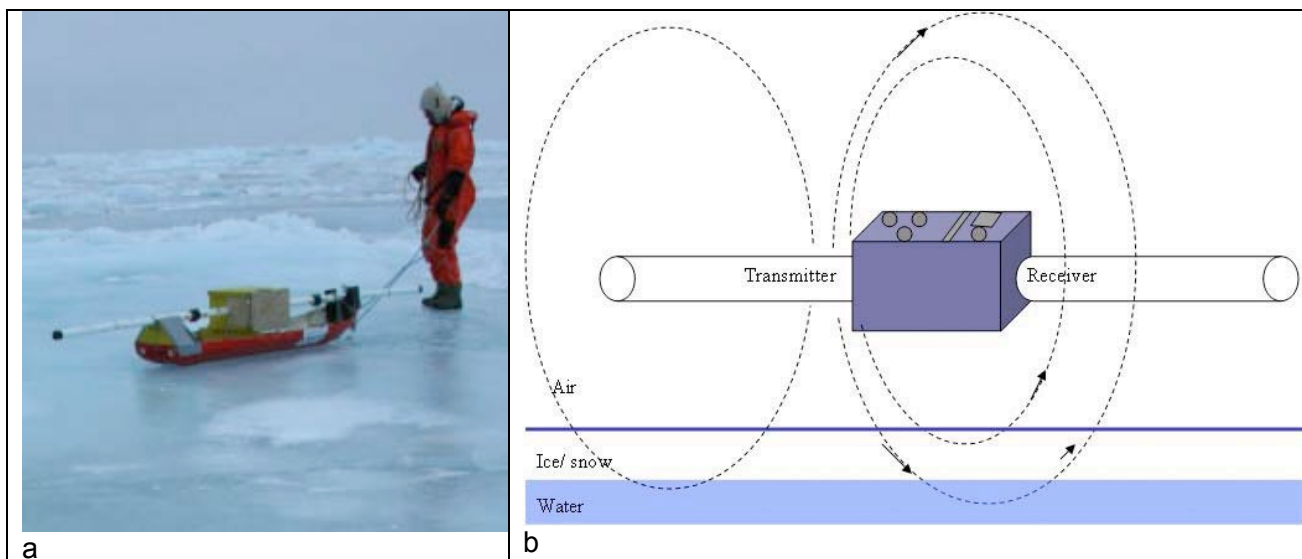


Figure 3.3. (a) Picture of the EM-31 instrument mounted on a sledge; (b) the principles of the electromagnetic induction method used to measure ice thickness. The lines are eddy current loops, which generates a magnetic field proportional to the value of the current flowing in that loop. The receiver receives the signals as voltage and can from that find the conductivity in the penetrated material.

On the cruise the EM-31 instrument was used to measure ice thickness. Three cross-sections each with a length of 100 m were made in the following way; First the thickness was measured with the EM-31 ICE which was put down on to the snow every 5 meters. Afterwards the freeboard, ice thickness and snow depth were found by drilling holes through the ice and measure the thicknesses with a ruler at the same locations. Two of the cross-section were made in St. Jonsfjorden and the last on an ice floe, a total of 63 comparative measurements. In addition to these three cross-sections, the ice thickness of two ice floes was investigated with the EM carried in hip height.

The EM-31 works in the way that it sends out electromagnetic signal at a frequency of 9.8 kHz at one end of the instrument and resaves these signals at the other intercoil spacing is 3.66m

(Fig.3.3 b). Electromagnetic wave propagation depends on the properties of the material the waves propagate through, conductivity is one such parameter. The EM-31 utilizes this and uses the difference in conductivity of different layers to find the thicknesses (Geonics Ltd, manual). The EM-31 ICE is specially designed for use on ice and take advantage of the fact that ice has a conductivity that is considerably lower than that of saltwater.

According to the MANUAL the EM-31 should be able to measure the ice-thickness with an accuracy of 5% if the conductivity is 20mS/m. During the days in St. Jonsfjord we found that a 0,1simens/m difference in pre-inputted conductivity leads to a 2cm difference in the output data, which means that this instrument is quite sensitive to the conductivity input if the thickness on the cm level is preferred. To get accurate measurements it is therefore necessary to find the conductivity at each place. In St.Jonsfjord and at the ice floes the conductivity was rather stable so we used the same conductivity for the entire 100m measurement, On the first day, the conductivity was set to 2,7 and it did turn out to be 2,8, so the data in the North-South direction is corrected by 2 cm.

The EM-31 measures the distance from the instrument to the seawater, and does not distinguish between ice, snow and air. This means that to find the ice thickness the distance from the device to the surface and the depth of the snow must be taken in to account. The system is constructed so that it measures with satisfactory accuracy at a hip height above ground (Geonics manual). From the data collected on St. Jonsfjorden and on the first ice floe, comparison can be made between the EM measurements and the manually found results from the drillholes. The upper part of Figure 3.4 presents the ice, snow and freeboard thicknesses that were measured during the cruise. The EM measured thicknesses are also plotted. The measurements from the ice floe can clearly be recognized by the thicker and more variable ice. North-South (NS) of the fjord represent the direction across the fjord, while East-West (EW) is perpendicular to the fjord. The first day the NS measurement was conducted, the second day the EW direction were investigated.

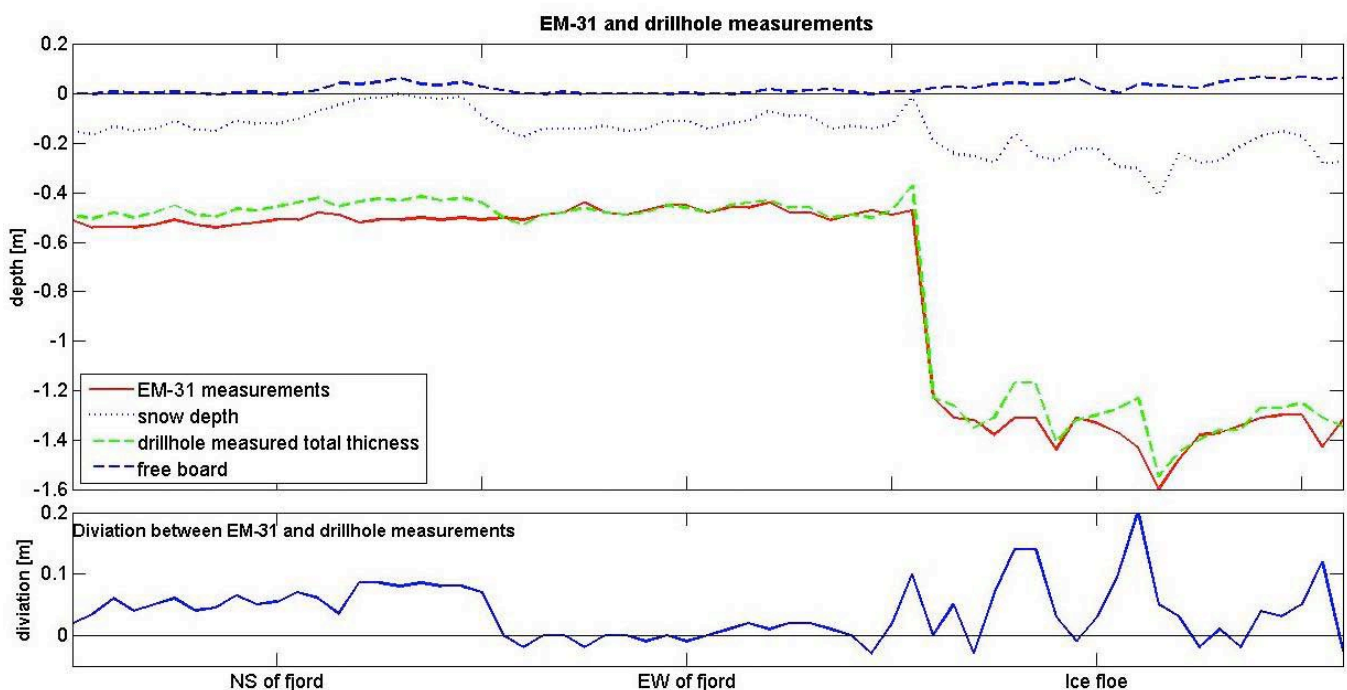


Figure 3.4: Horizontal section of all the calibration measurements that were conducted during the cruise. The zero line in the first figure is the surface of the snow.

The EM-data in the EW direction of the fjord are corrected for the error caused by the instrument sinking down in the snow. The error is of a magnitude from 0-3cm. On the first day on the fjord and at the ice floe no such measurements were made, so it is not possible to do the same correction here. On the first day the conductivity of the EM- were set to 2.7, but was later proved to be 2.8 so the EM data for NS are corrected with 2 cm in retrospect. The lower part of Figure 3.4 shows the difference between EM and drillhole measurements. It can be seen that the deviation between the drillhole and EM measured thicknesses are less than 0.2 meters at the ice floe and less than 0.1 meter in the fjord.

The values for the ice thickness obtained from Archimedes' law are shown in table 3.2. The different thicknesses that were measured are also displayed. The thickness values are found from the averages at each location where comparable measurements were performed. The density for wind packed snow were set to 350kg=m3. The seawater density is found to be 1027kg=m3 from the CTDs taken in St.Jonsfjord. The density value for the ice is 945kg=m3 which is the average value from the ice cores drilled during the course. The calculated Archimedes gives higher values for the thickness than what are measured at all three locations. From the table it can be seen that the ice at the ice floe is more than twice as high as the ice in the fjord, and that the deviation from the average is three times as high there.

Table 3.2: The measured thicknesses at the three comparing sections, and the thickness found from Archimede's law. The carrying capacity of snow on the ice is found from Archimedes' law to be 0,23 of the ice thickness. The ± gives the standard deviation in meters

	NS-fjord ice	EW-fjord ice]	ice floe one
average thicness EM	0.52m±0.02	0.46m±0.02	1.36m±0.08
average thickness drillhole	0.47m±0.03	0.47m±0.03	1.31m±0.09
average snow depth	0.09m±0.06	0.12m±0.03	0.34m±0.06
average free board	0.02m±2.08	0.006m±0.71	0.04m±1.80
average ice thickness drillhole	0.37m±0.03	0.35m±0.01	1.07m±0.07
Ice thicness using arcimedes	0.63m	0.59m	1.94m
carrying capacity of the ice	0.08m snow	0.08m snow	0.25m snow
conductivity of sea water	2.8	2.7	2.7

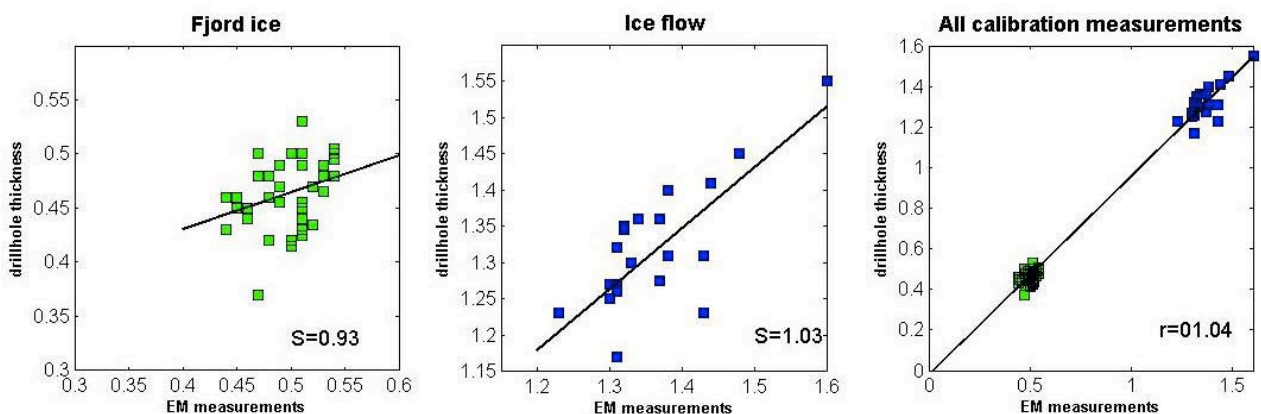


Figure 3.5: Scatterplott of drillhole measurements vs EM measured thickness. S is the slope of the regression line

From the scatter plots in Fig. 3.5 the relationship between EM measured thickness and the drillhole determined thicknesses is plotted to better see the relationship between them. A total of 63 comparison measurements were performed. The drillhole thickness is the total of both the snow and ice thickness in these cases. In table 2 the different results from the comparative calculations performed on the data are listed. The regression line and correlation coefficient are found using standard matlab functions. The correspondence between the measurements methods increase when the number of measurements increases, and for all the comparative measurements the correlation coefficient is 0.99. Figure 3.6 and 3.7 display the thicknesses distribution at the first and second ice floe, these thicknesses are the combined thickness of the ice and snow, as no direct measurements of the snow depth were made. The length from the EM, carried in hip height, to the ground is subtracted. On the last measurement conducted on the first ice floe, the battery voltage of the instrument went down sharply, leading to possibly to high results for the NS measurements at 35m line. These values are not shown in the plots 69 to better see the general situation.

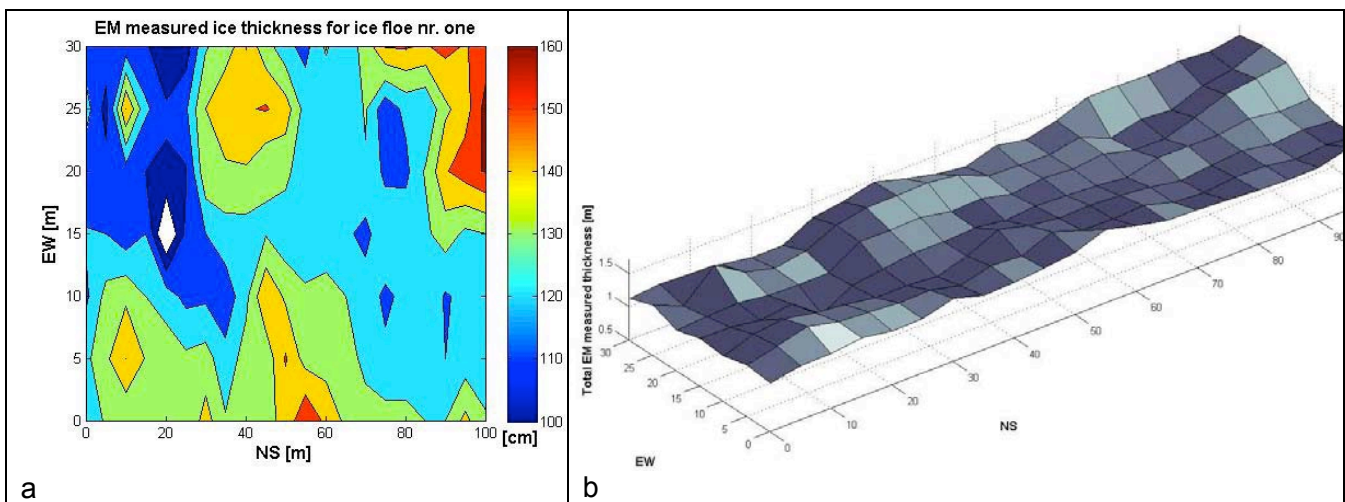


Figure 3.6: EM measured ice thicknesses at the first ice floe. The first is the ice as seen from above, and the second is the same shown in 3D

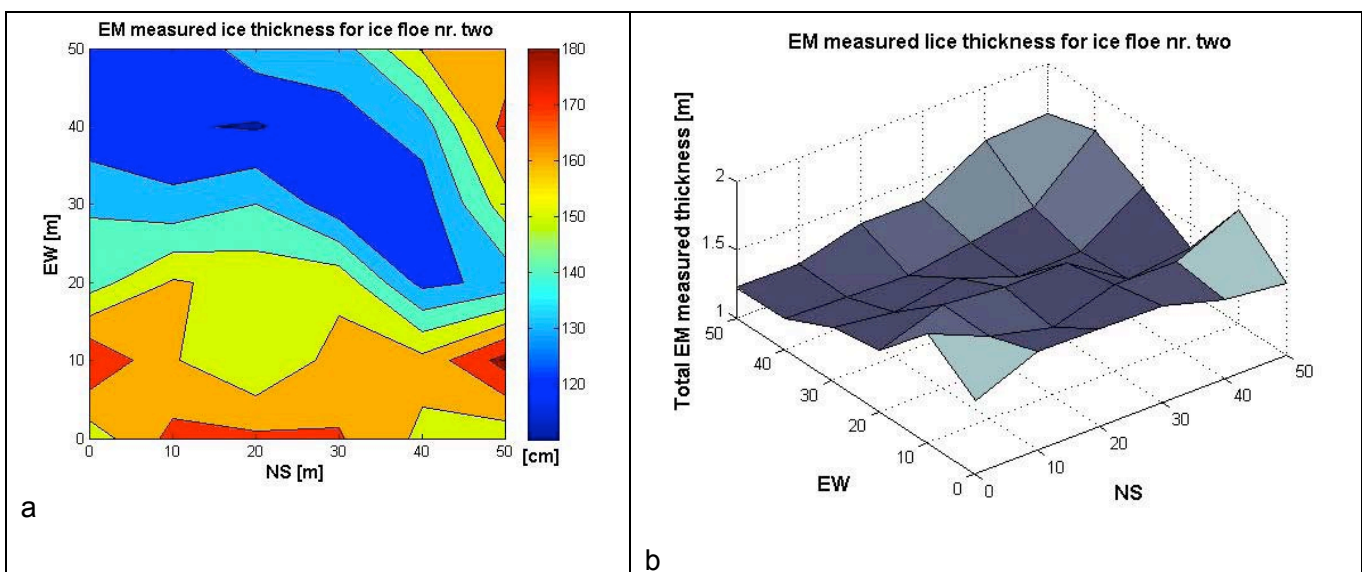


Figure 3.7: The same as in Figure 3.6, but for the second ice floe

In Figure 3.8, the distribution of the ice thicknesses from the collected data can be seen. In the histogram from the first ice floe the measurements with a critical battery level are included, but they might as stated earlier in this section be to high values. The thickness at ice floe nr. 1 varies between 0.8m and 2.5m, at the second ice floe it varies between 1.1m and 1.9m. The ice in the fjord is much thinner and with a smaller variation, between 0.43m and 0.55m.

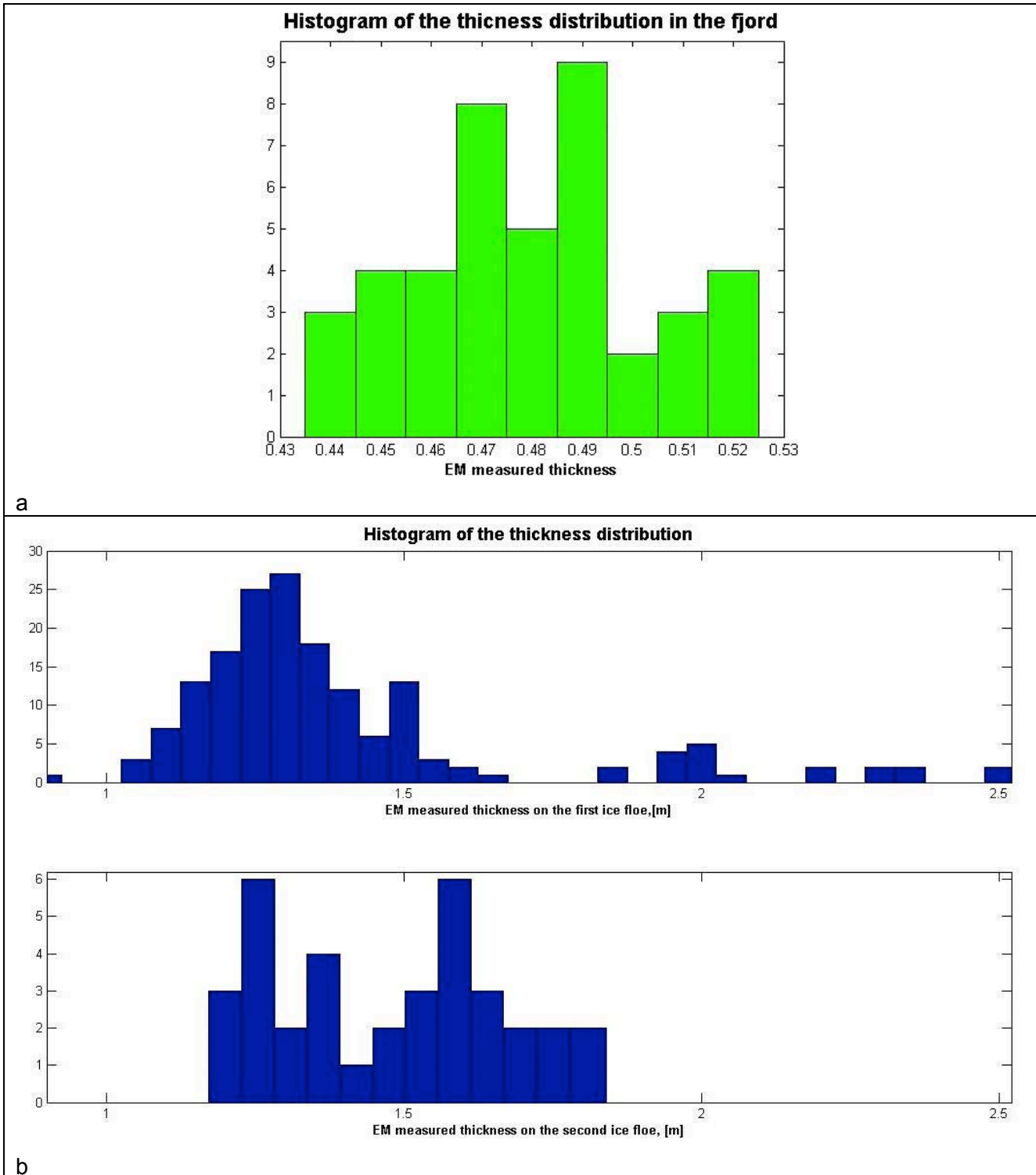


Figure 3.8: Histogram of the ice thicknesses in St.Jonsfjorden, and at the ice floes.

Table 3.3: Comparisons between EM and drillhole data

	Ice floe	NS and EW of the fjord	all three combined
Average thickness EM	1.36m	0.50	0.78m
Average thickness drillhole	1.31m	0.46	0.75m
Average differens EM - drillhole	0.05m	0.04m	0.03m
Slope of regresion line	1.03	0.93	1.04
Correlations coefisient	0.75	0.29	0.99

The EM measurements have been compared with the drillhole measurements. The correction for the use of a too low value for sea water conductivity on the first day, leads to a bigger difference between the EM-measurements and the drillhole founding. This is unexpected, and it can be questioned whether it is reasonable to correct the numbers in retrospect. The data from the first day is not corrected for the instrument sinking down in to the snow either, such a correction would lead to an even bigger error. However this error is small, and when all the comparable measurements are taken in to account the EM measured and manually found thicknesses seems to correspond very well. The ice in the fjord shows small variations in thickness over the cross sections, so the spread in the data is too narrow to give a good enough correlation based on only these measurements. On the ice floe the spread were bigger but the number of measurements was too few to get a statistically significant picture of the correlations. A measurement size of more than 30 is needed for a statistically valid comparison (Emery et.al 2004). When all the comparing measurements are taken into consideration, they seem to correspond very well. The correlation coefficient for all the 63 measurements is 0.99, meaning that it is highly likely that they measure the same population.

From the grid measurements made with the EM31 at the ice floes, the thickness of the ice varies quite much. It varies between 2.5 and 0.9 meter for the first ice floe, on an area of 3500 m², and between 1.8 and 1.2 on the 2500m² for the second one. The EM31 receives signal as voltage, meaning that a lowering of the battery capacity can contaminate the results. The low battery voltage on the last measurements from ice floe one could therefore be the reason for the much higher values for the thickness, than was the case for the rest of the grid. However, a small ridge was observed on the surface, and from theory it is known that only 10% of a ridge will be situated on the surface (Marchenko, 2010), such that even a small ridge on the surface can be followed by a deep keel on the bottom of the ice. Unfortunately the ice floe cracked before we were able to walk the line again with a fully charged battery.

As it can be seen from the plot of the three cross sections (Figure 3.5), the ice in the fjord is much more uniform than the ice on the ice floe. In the fjord the ice has been able to grow thermodynamically with only small disturbances from wind and waves, in contrast to the ice floe, where the ice shows a greater impact from dynamically deformation during the growth. This leads to a much larger variation in sea ice thickness on the ice floes (Figure 3.6). On the ice floes the measurements were made on a relatively plain surface, but the ice floe as a whole had a much greater range in thickness, this due to a lot of ridge formation on the rest of the floe. On the fjord the ice seemed uniform in thickness also outside of the measurement area. So the thickness range would likely show even more deviation if bigger areas were examined.

The ice and snow measurements from the fjord are plotted again in Figure 3.8 to get a better impression of the snow and ice relations. The figure shows a negative correspondence between the snow depth and ice thicknesses, this leading to a zero or negative freeboard were the snow thickness is largest.

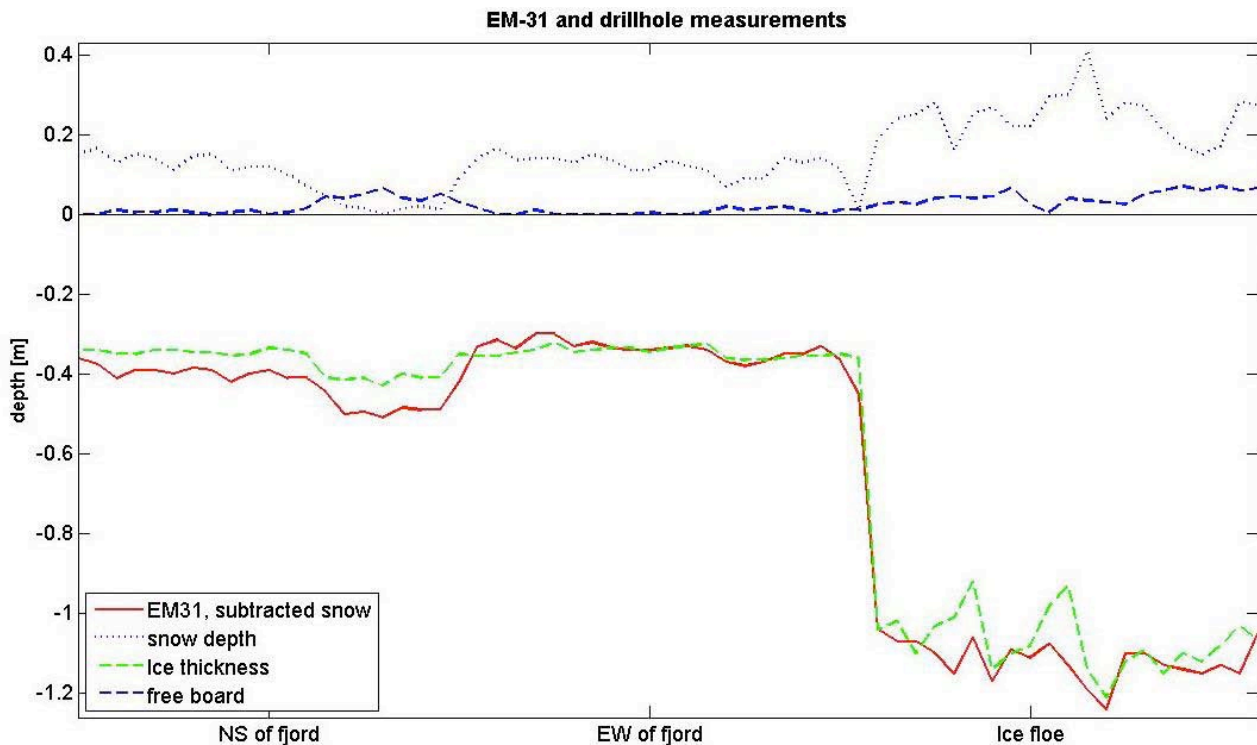


Figure 3.9: The measurements from the calibration, plotted with the ice surface as the zero level. The snow depth has been subtracted from the EM data.

The negative correspondence is probably due to the insulating effect of the snow cover. The heat conductivity of the snow is a lot smaller than that of ice, so the latent heat released during the freezing of water can not be transported as fast through the ice as if no snow cover were present (Lepparanta, 1991). The same is not so evident for the ice floe. This might be due to the fact that other mechanisms than just thermo dynamical growth has been participating here. However it was observed a layer of refrozen snow on top of the ice, suggesting that the ice has been subjected to a flushing event. If the free board is negative the seawater will start to percolate through the ice, and freezes on the bottom of the snow. This refreezing will make the ice grow faster as described by Lepparanta (1991). This might be the reason for the observation of thick ice despite the snow cover. The freeboard in the fjord and at the ice floes were several places found to be negative, this happens when the snow cover is too heavy to be held up by the buoyancy of the ice. If the ice thickness is less than 2.3/three times the thickness of snow, the freeboard will be zero or negative. According to the measurements performed on the ice floe and in the fjord the snow amount is close to what the ice can carry on average, leading to a negative freeboard where the snow thickness is higher than average, and the ice thickness correspondingly smaller.

The calculations using Archimedes principle give an ice thickness that is up to half a meter higher than what is observed. The formula is quite sensitive to small changes in the density values. So to get a better comparison more accurate numbers would have been preferred. In the calculation only the average values are used. The freeboard was in general found to be very small, and some times also negative, but with some higher values in between, these higher values might have created a too big freeboard in the average. If the freeboard is set to zero in the formula, which is more in line with the observations on the ice, the calculated thicknesses would be 0.33 in the NS and 0.51 for the EW on the fjord ice, and 1.44 for the ice floe. This agrees better with what is found from the EM measurements and the drillholes. In general the ice thickness that were measured during the cruise goes well with theory, with the most varying and thickest ice on the ice floes, and a thinner and more uniform ice covering the fjord. The insulating effect of the snow cover and the maximum carrying capacity of the ice can also be seen from the measurements.

Data collection by NPI

During several cruises in the Fram Strait and Barents Sea area, CryoSat-relevant data (sea ice thickness, snow thickness, freeboard, ground electromagnetics with Geonics EM31) were collected along with the longterm sea ice monitoring work of the NPI. Work was done on a number of ice stations, where the EM31 instrument was mounted on a sledge along with a small computer and GPS receiver to record automatically continuous thickness data.

The CryoSat-2 calibration and validation-relevant in situ datasets collected by the Norwegian Polar Institute (NPI) on the snow and sea ice characteristics presented in Forsström and Gerland (2009) are from years 1999 - up to 2008. The main field area is Fram Strait, between Greenland and Svalbard, where both autumn (2004, 2006, 2007) and spring (2005, 2007, 2008; see e.g. Gerland et al. 2006) data were collected during cruises with the research vessels "Lance" and KV "Svalbard". Besides this, a dataset collected in the Barents Sea (1999) area was also included. See Figure 3.9 for the map over the field sites.

The dataset consists of in situ drill-hole measurements of ice, snow and freeboard thicknesses. Ice densities from sea-ice cores and snow densities from pit studies are also included. The data were collected during several spring and autumn field campaigns in the years 1999–2008. Landfast sea ice in Spitsbergen fjords, coastal sea ice of Svalbard and drift ice in Fram Strait and the Barents Sea (Fig. 3.9) are all included. Typically at an ice-station site, a snow-pit study is conducted to provide the vertical stratigraphy, temperature and density profiles in the snow on the sea ice. Ice coring for temperature, salinity, chlorophyll content and, often, for density are conducted. Thickness drilling transects including snow depth, sea-ice thickness and freeboard measurements, spanning up to 500m in length, are performed. The typical interval of drillings along a transect is 5–35 m. Each ice station consists of 1–31 (typically 5) measurements of ice and snow thicknesses. The location and orientation of the transects are chosen to be the most representative of conditions on the floe. Naturally, the regions of thinnest ice are not investigated since the ice must be thick enough to safely work on. Also, the limited number of drillings might not capture the thickness distribution over the whole floe. For further calculations the data are averaged over an ice floe site, which means averaging over the scales of 10–500m.

The actual thickness reading has an uncertainty of 1 cm. The thickness drillings are conducted using, typically, 5–10 cm diameter drills. For ice density, the core pieces, typically 10 cm long, are weighed and the mean density for the site is calculated as an average weighted by the length of each core piece. Sea-ice density measurements made by weighing the core are often subject to a negative bias due to the loss of some of the brine content and deviation from the ideal form (in this case cylindrical) of the sample (Timco and Frederking, 1996). The uncertainty in the density measurements is $\pm 15 \text{ kgm}^{-3}$. For snow density, a known volume (0.5 dm^3) of snow is collected using a density probe inserted horizontally into the wall of a snow pit, and then weighed. The measurement is repeated along a vertical profile through the snowpack. A weighted average based on the measurement depths is calculated to obtain the mean density through the snowpack. For snow density measurement, the largest cause of bias is the difficulty in filling the density probe without compressing or losing any snow. The estimated uncertainty for ρ_s measurement is $\pm 50 \text{ kgm}^{-3}$.

The relevant parameters included in the study here are snow thickness, ice thickness and freeboard (all measured in drillholes on sea ice stations), as well as ice density from core samples, and snow density from snow pit studies (tube measurements). The data were used for intercomparison with corresponding historical data (Forsström and Gerland 2009), and for assessing the role of the different parameters when calculating sea ice thickness from altimetry measurements Forsström and Gerland 2009, Forsström et al. 2011). For the calculation of ice thickness from altimeter freeboard measurements, knowledge or at least realistic estimates about snow thickness and snow and ice density are necessary.

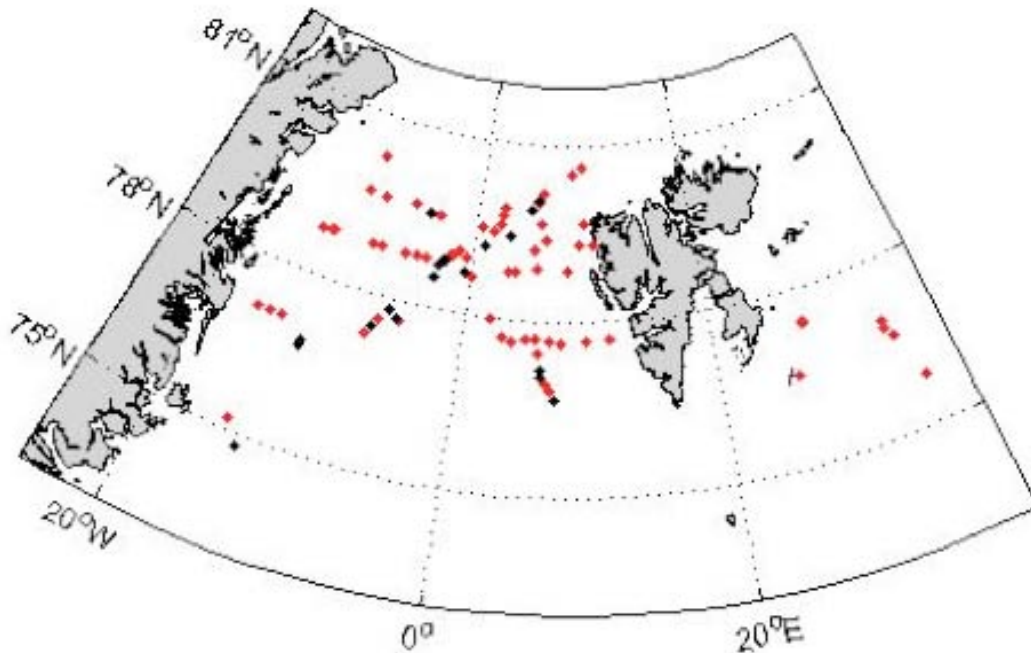


Figure 3.9: The NPI snow (red markers) and sea ice density (black markers) field sites on Fram Strait and Barents Sea. Data collected 1999 – 2008. From Forsström and Gerland (2009).

The sea ice in Fram Strait contains ice of various ages transported south from the Arctic basin, as well as some locally formed young ice. Therefore the h_i is relatively broadly distributed over the thickness range (Fig. 3.10 b), whereas for the landfast ice around Svalbard and the ice in the Barents Sea (Fig. 3.10 a), the PDF is skewed toward the smallest h_i . The average h_i for Fram Strait is 2.35m (averaged over both seasons), whereas for Svalbard and the Barents Sea it is 0.63m. The measurements in Fram Strait can be considered representative as they compare well with the earlier reported thicknesses from Fram Strait (Vinje and others, 1998, table 3).

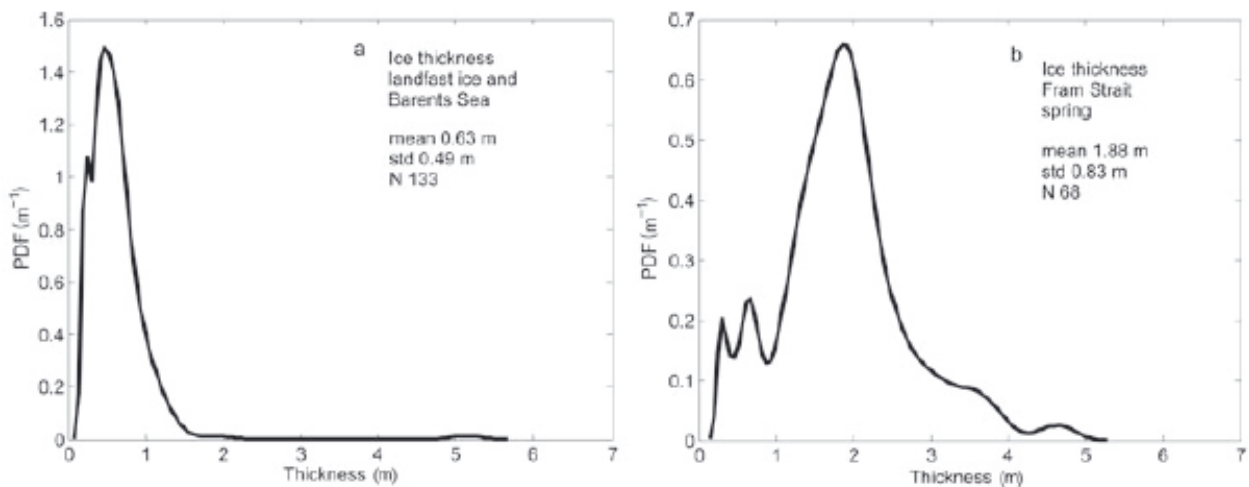


Figure 3.10. PDFs for sea-ice thickness data pooled for the Barents Sea and Fram Strait.

Despite the small number of data points, the thickness drilling data from the Barents Sea compare well with the drafts reported by Abrahamsen and others (2006) from mooring upward-looking sonar measurements in the years 1995–96. In the comparison, one needs to account for the thinnest ice, missing in the in situ data. In 1995, the mean draft was +0.5m thicker and in 1996 it was very similar to our measurements in 1999. As pointed out by Abrahamsen and others (2006), sea-ice conditions in the Barents Sea can experience large interannual variability. The autumn ice thickness data are sparse compared with the spring dataset and are dominated by multi-year ice. No thin first-year ice is present in the autumn data, and therefore the average thickness is >3m. For spring the average h_i is <2m.

Table 3.4. Ice thickness, h_i (cm), freeboard, h_f (cm) and density, ρ_i (kgm^{-3}). N is the number of measurements (stations) in this study 1999–2008. The measurements are averaged over an ice station before calculating the mean and the standard deviation (std)

	Month											
	Aug.	Sep.	Oct.	Nov.	Dec.	Jan.	Feb.	Mar.	Apr.	May	Jun.	Jul.
N	16 (5)	121 (38)	0	0	0	30 (19)	61 (19)	81 (24)	232 (53)	624 (74)	39 (10)?	2 (2)
h_i mean	347.5	304.1	–	–	–	43.1	58.2	71.8	133.6	125.7	87.6	123.0
h_i std	57.0	128.0	–	–	–	20.0	21.1	26.5	80.5	108.3	44.9	99.0
h_f mean	36.5	29.8	–	–	–	-1.0	1.4	12.5	9.7	8.0	2.8	8.5
h_f std	10.0	15.4	–	–	–	5.3	4.0	33.5	12.4	14.0	4.5	7.8
N	0	11 (8)	0	0	0	0	0	0	7 (6)	10 (7)?	1 (1)	0
ρ_i mean	–	899.9	–	–	–	–	–	–	892.8	909.7	903.8	–
ρ_i std	–	17.6	–	–	–	–	–	–	18.9	26.9	0	–

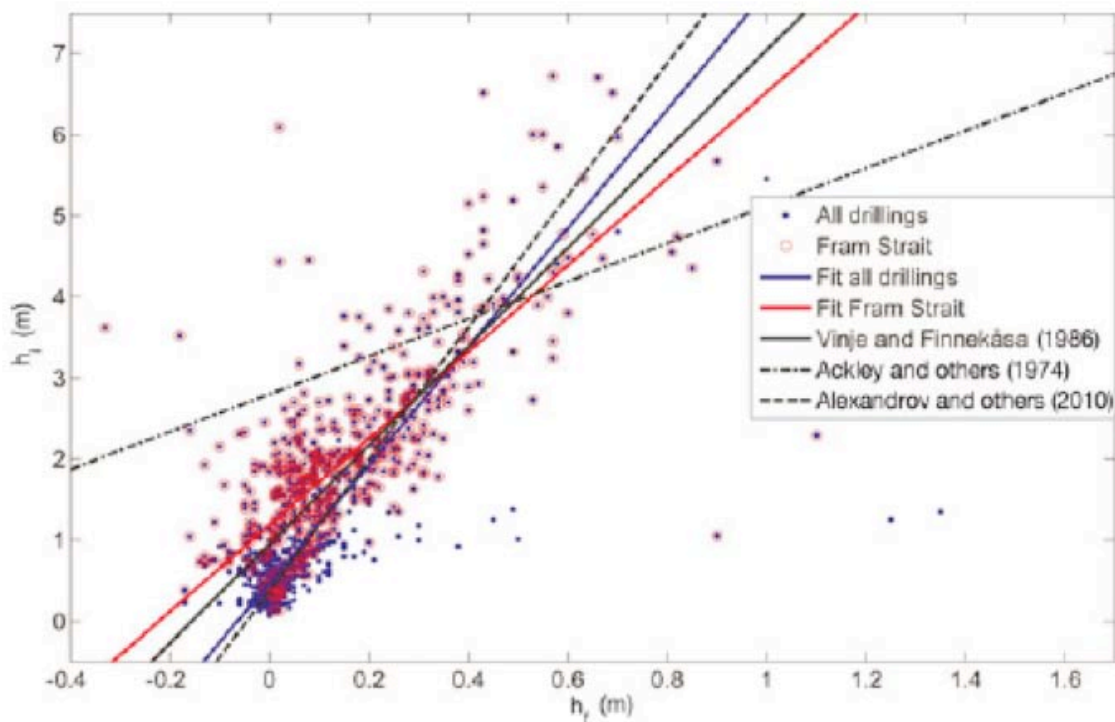


Figure 3.10: In situ ice thickness as a function of freeboard (dots denote all drillings from Forsström et al. (2011), circles drillings in Fram Strait), together with linear robust fits ($h_{\text{fit}} = 7.37h_f + 0.44$ (m) and $h_{\text{fit}}(\text{FramStrait}) = 5.34h_f + 1.19$ (m)) The black lines are previously published relationships from corresponding in situ data. Many factors, such as the fitting method, the location, timing and method of measurements, differ from those used in Forsström et al. (2011).

A more detailed view of the seasonal evolution of h_i , h_f and ρ_i , independent of year and region, is presented in Table 3.4. The thickness maximum due to thermodynamic growth is reached in late spring, which shows up as a sub-maximum of h_i in April–May. Similar timing for the h_i maximum in Fram Strait is reported by Vinje and others (1998). They observed the ice thickness minimum to occur in September, which in our dataset, on the contrary, is during the season with the greatest thickness. Linear robust fits between h_f and h_i from the thickness drilling (Fig. 3.9) correspond very well with the work of Ackley and others (1976), Vinje and Finnekåsa (1986) and Alexandrov and others (2010). Figure 3.10 demonstrates the difference between regions in the Arctic Ocean, as the two datasets collected in the Fram Strait area (Vinje and Finnekåsa, 1986, and this study) are more congruent to each other than to Alexandrov and others (2010) and Ackley and others (1976), whose data are from the Russian Arctic and Beaufort Sea, respectively. The results reported by Vinje and Finnekåsa (1986) were obtained from 382 drillings on level ice (not on ridges) during summer months (July–August, 1981–84). Despite the difference in the timing and method, their slope and ours compare well. The initial density of the sea ice depends on the conditions whilst freezing. The change in the volume fraction of brine and gases is the mechanism through which ρ_i decreases in growing and ageing ice. This evolution appears only weakly when plotting ρ_i against h_f (Fig. 3.11). The ice density data consist of both first- and multiyear ice in 29 ice cores from Fram Strait, with an average column density of 901.9 kg m^{-3} , which is lower than the mean of previously reported values (910 kg m^{-3} ; Timco and Frederking, 1996). Fram Strait ice contains some thin newly formed ice, but has a large fraction of multi-year ice. This explains the low densities and perhaps also the relatively high variability (standard deviation between the ice stations 22 kg m^{-3}). Generally, the variability of ρ_i can be expected to be an order of magnitude smaller than that of ρ_s .

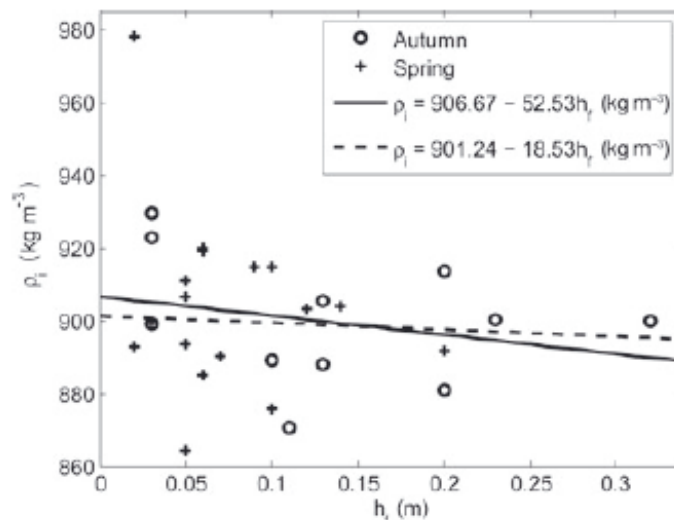


Fig. 3.11. Sea-ice densities as a function of freeboard for 29 cores from Fram Strait, 2005–08. The linear fit (solid line) is strongly influenced by the exceptionally high data point in the lower part of the h_f range. Applying a robust linear fit (dashed line) yields a weaker dependence between ice density and freeboard.

A comparison of measured and calculated ice thickness (using hydrostatic equilibrium equation) is shown in Fig. 3.12. The absolute deviation between the measured and calculated thickness in Fram Strait is, on average, 49 cm (23% of measured h_i). In the case of thin first-year ice created by thermodynamic growth without significant dynamic disturbance, the calculated ice thickness mimics the measured one well (Fig. 3.12 a). The deviations between the measured and calculated h_i increase slightly toward the thicker part of the thickness range, where the dynamics play a more prominent role. On ridged multi-year ice a larger number of drillings is needed for a representative picture of the thickness distribution. The peaks in Figure 3.12a indicate the cases

where drillings were conducted close to or at a pressure ridge. Due to the thinner ice along the Svalbard coast and in the Barents Sea, the deviation from the hydrostatic equilibrium assumption is more critical for their thickness estimate than in the case of the thicker ice in Fram Strait. The measured and calculated ice thicknesses for the Svalbard coast and Barents Sea differ by 36 cm, on average, which is less than three-quarters of the deviation in Fram Strait, but is 48% of measured h_i in the area. Purely thermodynamic ice development occurs rarely, but snow-to-ice transformation (Nicolaus and others, 2003; Gerland and others, 2004) complicates the ice evolution and makes the differentiation of snow and ice more convoluted. The landfast ice sites located in protected fjords (Krossfjorden and Kongsfjorden, Svalbard west coast, are often protected from strong winds and large-scale drift ice motion. Therefore the calculated h_i mimics the measured h_i better for the Svalbard landfast sites and the Barents Sea than for Fram Strait (Fig. 3.12). However, a small absolute error is of more importance for thin coastal ice than for thick ice in Fram Strait. The proximity of the shore and the shallowness of the water bring about particular dynamics affecting the ice freeboard. An example is a situation experienced at Hopen where the ice packed toward the shoreline by winds was resting on the bottom (Gerland et al. 2008a). In cases like this (the rightmost values in Fig. 3.12 b), the ice freeboard is not determined by the water buoyancy, so the difference between the measured and calculated ice thicknesses becomes much higher than in cases of pressure ridges (Fig. 3.12 a). This situation is exceptional and occurs only in locations shallower than the draft of the drift ice.

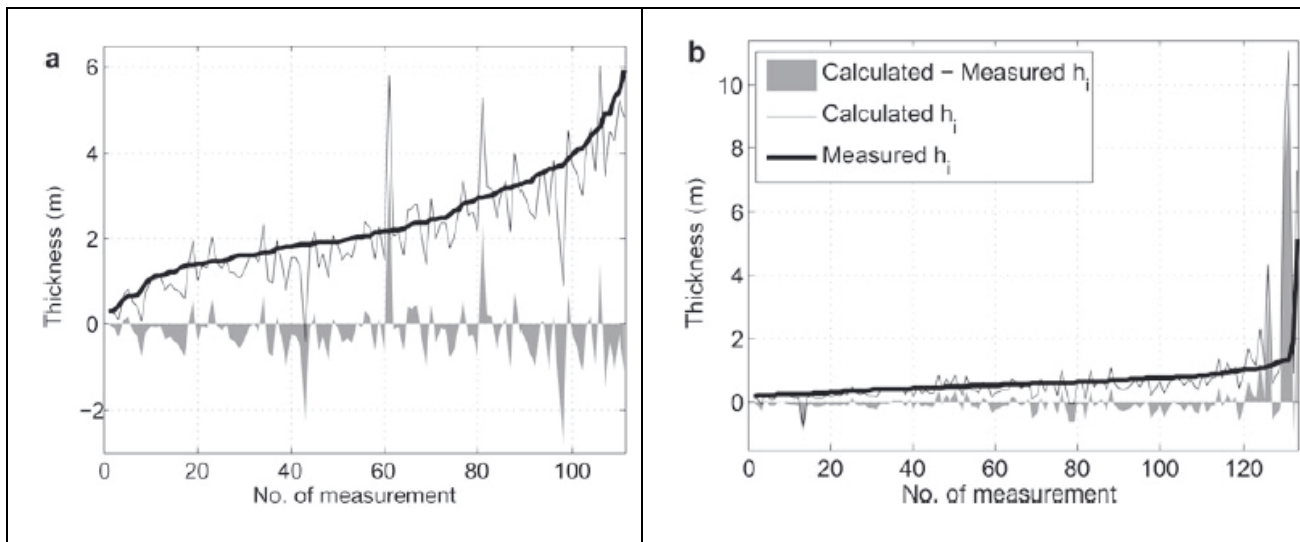


Fig. 3.12. The measured sea-ice thickness (thick curve) and the ice thickness calculated assuming hydrostatic equilibrium (thin curve) for (a) Fram Strait and (b) the Barents Sea and the landfast sea ice at the Svalbard coast. The in situ measured snow and freeboard thicknesses averaged over an ice station (scales of 10–100m) are used for calculation. The sea-water density was set to 1024 kg m^{-3} and the snow and sea-ice densities to the averages of the data in this study. The grey area shows the difference between the measured and calculated ice thicknesses. In both graphs the data are sorted by measured ice thickness.

Snow conditions

The snow measurements from this study are compared with the climatology of Warren (1999) (Table 3.5). Our study area being south of the region covered by the climatology, differences in climatic conditions between the NP-stations in Warren (1999) and the sites of the present investigation are likely to be significant. Table 3.5 shows the h_s , ρ_s and snow water equivalent calculated for different months, independent of year. It is apparent that the data are collected during several field seasons at various locations instead of monitoring the snowpack evolution at one site.

Table 3.5 Snow thickness, h_s (cm), density, ρ_s (kgm^{-3}), and water equivalent, SWE (cm), compared with the quadratic fit of the snow climatology by Warren and others (1999) for the whole Arctic, 1954–91. N is the number of measurements (stations) of this study, 1999–2008. The h_s measurements are averaged over an ice station before calculating the mean and standard deviation (std). For ρ_s and SWE, only one measurement per ice station was conducted

	Aug.	Sep.	Oct.	Nov.	Dec.	Jan.	Feb.	Mar.	Apr.	May	Jun.	Jul.
N	16 (5)	121 (38)	0	0	0	30 (19)	61 (19)	81 (24)	232 (53)	624 (73)	39 (10)	2 (2)
h_s mean	7.7	8.4	–	–	–	17.5	18.9	14.7	24.2	17.0	14.1	11.0
h_s std	3.2	5.7	–	–	–	11.5	11.4	11.8	20.5	16.0	15.5	11.3
h_s War99	3.0	11.2	19.4	23.0	24.9	27.1	29.7	32.4	33.7	34.4	30.7	6.6
N	0	2 (2)	0	0	0	0	2 (2)	0	28 (28)	29 (29)	2 (2)	0
ρ_s	–	296.3	–	–	–	–	368.5	–	294.0	280.9	346.5	–
ρ_s std	–	89.0	–	–	–	–	2.1	–	63.7	45.0	53.0	–
SWE mean	–	4.0	–	–	–	–	15.1	–	10.0	7.8	10.2	–
SWE std	–	3.3	–	–	–	–	0.1	–	7.8	6.1	1.8	–
SWE War99	0.7	2.7	5.2	6.6	7.3	8.0	9.2	10.3	10.6	11.0	10.4	2.4

Figure 3.13 shows the PDFs for the observed snow thicknesses. Snow thicknesses in the autumn average 8 cm (Fig. 3.13 left), whereas the spring snow layer on the sea ice is 19 cm thick on average. As Fig3.13 shows, the Fram Strait sea-ice h_s varies greatly (std dev. 19 cm); this is due to the wind redistribution on an uneven surface. As the sea ice in Fram Strait originates from different regions in the Arctic, the different floes have different weather histories, which is one cause of variability. On the landfast sea ice and the Barents Sea the snow cover is notably thinner ($h_s = 13$ cm on average), and varies less than on the Fram Strait ice, most likely due to the even ice surface and shorter accumulation season. The spring h_s in this study are significantly lower than those found by Warren (1999) in the central Arctic (Table 3.5) during 1954–91. The difference is largest for the months with highest h_s and less pronounced in the autumn data. Potential explanations for lower h_s in our data could be the warmer locations, implying more melting and (together with thinner ice) more snow-to-ice transformation.

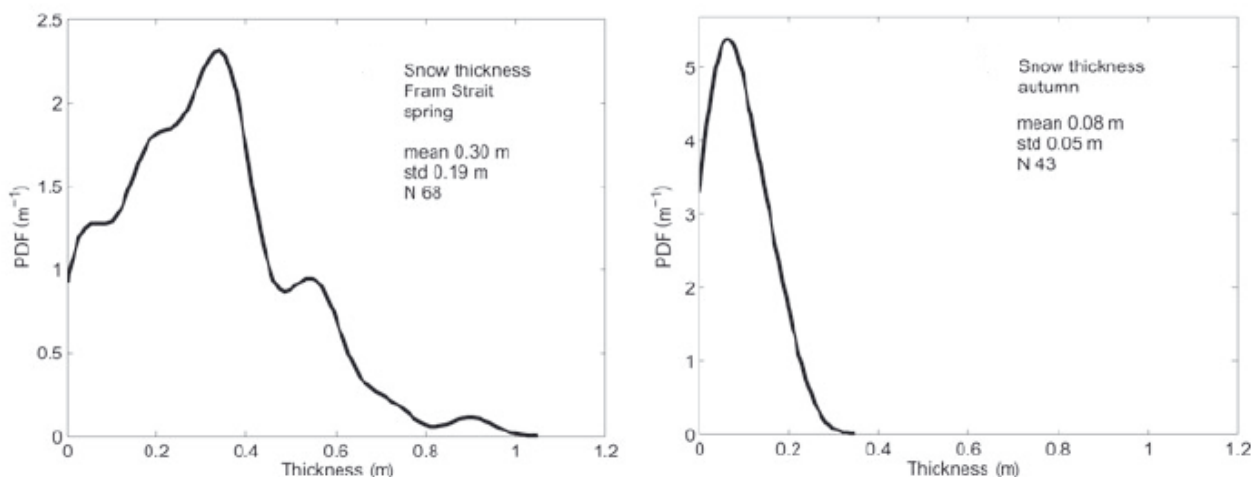


Figure 3.13. PDFs for the observed snow thicknesses in the Fram Strait. A smoothing window of 0.05 m is applied to the data.

The column snow densities average 292.5 kgm^{-3} (relative std dev. 0.2), which compares closely to the annual average of 300 kgm^{-3} over the Arctic basin reported by Warren (1999) increasing from 250 kgm^{-3} in September to 320 kgm^{-3} in May. Besides this seasonal variation, they reported that ρ_s exhibited little geographical variation across the Arctic. The small-scale variation of ρ_s , typical for snow parameters due to various depositional (wind and humidity conditions during snowfall) and post-depositional processes (redistribution by snowdrift, snow metamorphosis), is apparent in our data.

Conclusions

The distributions of the sea-ice thickness and snow depth measured in situ, mostly in Fram Strait, and also the Barents Sea and Svalbard coast, are presented. The measured h_i distributions compare well with earlier published work. The h_s is significantly lower than the values presented by Warren (1999) snow climatology for the Arctic basin. The in situ drilling data averaged spatially over 10–500m are used to estimate the degree to which the assumption of hydrostatic equilibrium, used in the sea-ice thickness calculation from altimeter data, holds. The hydrostatic equilibrium assumption holds reasonably well for most of the landfast ice, but is less accurate for drift ice. However, for thin ice the relative errors are more prominent than for thick drift ice features in Fram Strait. The deviation between the calculated and measured thickness was on average 49 cm (23% of measured h_i) for Fram Strait and 36 cm (48% of measured h_i) for the Svalbard coast and Barents Sea. The measured snow densities compare well with the Warren (1999) climatology. The sea-ice densities presented large variability and were lower (901.9 kgm^{-3} on average) than literature values (Timco and Frederking, 1996; Kovacs, 1997), resulting from the large portion of light multi-year ice included in the present study. Given the measured spatial variability of the snow and ice parameters, the uncertainty propagating to the calculated sea-ice thickness was estimated. The variability in ice density is found to be larger than previously reported, which brings about an uncertainty of 25 cm in the calculated ice thickness product. Based on our data the error in snow thickness is an even larger source of error (37 cm (radar) and 93 cm (laser altimetry)).

WP4: Report on IceSat data analysis

WP4: Analysis of selected IceSat laser altimeter data over different sea ice types such as multiyear, firstyear, new ice and open water

Use of IceSat altimeter data for sea ice thickness retrieval

The Geoscience Laser Altimeter System (GLAS) instrument on the Ice, Cloud, and Land Elevation Satellite (ICESat) provides global measurements of polar ice sheet elevation to discern changes in ice volume (mass balance) over time. Secondary objectives of GLAS are to measure sea ice roughness and thickness, cloud and atmospheric properties, land topography, vegetation canopy heights, ocean surface topography, and surface reflectivity. GLAS has a 1064 nm laser channel for surface altimetry and dense cloud heights, and a 532 nm lidar channel for the vertical distribution of clouds and aerosols. This level-2 altimetry product (GLA13) provides surface elevations for sea ice. Data also include the laser footprint geolocation and reflectance, as well as geodetic, instrument, and atmospheric corrections for range measurements.

The ICESat datasets contain nearly month-long observations of sea ice surface elevation and other radar characteristics for fall, winter, and spring periods covering the time period of winter 2003 to 2008 both in the Arctic and Antarctic region. The IceSat data have been used to determine the sea ice freeboard, or the height of the surface above the ocean level, to infer sea ice thickness using model estimates of snow depth on top of the floating ice (Kwok et al., 2007, 2008). These results have been used to estimate sea ice volume and characterize the changing thickness and volume of the Arctic Ocean sea ice system. Based on IceSat data, estimates of Arctic Ocean sea ice thickness from ICESat (Kwok et al., 2009) show a remarkable thinning of ~0.6 m in average ice thickness over a short period of four years between 2004 and 2008.

More information about ICESat at <http://icesat.gsfc.nasa.gov/icesat/>. ICESat data is available from NSIDC (<http://nsidc.org/data/icesat/index.html>)

Freeboard calculations

To measure freeboard correctly the local sea surface height have to be accurately known, but errors in e.g. the geoid model, tide models and effects of atmospheric loading will be present. According to studies by Kwok et al [2006], the standard deviation of sea surface error is approximately 38 cm after corrections for best available geoid, tides and effects due to atmospheric loading. This can be compared to the variability of the total sea ice freeboard of ~ 25 cm. One way of finding tiepoints is to use near-coincident SAR images to identify leads with open water along the ICESat ground track. These will provide an exact reference of the local sea level that can be used to calculate the local freeboard. This manual way of finding tiepoints for the local sea surface is however dependent on near coincident SAR images and is very time consuming [Kwok et al., 2006]. In a later article by Kwok et al [2007] acquired several hundred tiepoints manually with help from SAR images. They found a strong correlation between the manual tiepoints and the standard deviation of freeboard estimates averaged to 25 km grid cells. This relationship is used for statistically finding sea surface tiepoints, a faster method that gives much more data, albeit at a lower quality.

Processing of IceSat data

In the studies done at NERSC, IceSat GLAS data from the Fram strait was ordered from NSIDC, the data includes all operating periods from February 2003 to October 2007. Campaign 3H was chosen for a first look of the data, because of a good coverage of SAR images in this period. Some work has been done to implement the method provided by Kwok et al. [2006, 2007] to

calculate freeboard and estimate ice thickness, but no results are available for presentation at the moment. The parameters in Table 4.1 have been studied, both for individual orbits and for the campaign as a whole. Individual orbits have been co-located with a SAR image. This showed some promise for using sea ice roughness together with elevation for identifying older ice, both fast and drifting. Gain and reflectivity were good at identifying open water.

When studying the entire campaign 3H, data was binned into 25 x 25 km bins on a polar stereographic projection. If no data points were found in one bin, it was left empty, so no interpretation took place. If several data points were in the same bin, the mean was calculated. The surface roughness parameter (Fig. 4.1) shows that the fast ice at the Greenland coast is clearly visible as a blue band, indicating the lowest roughness. Next to this is a red-yellow band, where thick MY ice is dominant. Closer to Svalbard and open water the surface roughness decreases.

Table 4.1: ICESat data acquisition periods available at NSIDC

Laser ID	Start Date	End Date	Days
1	02/20/03	03/29/03	38
2A	09/24/03	11/18/03	55
2B	02/17/04	03/21/04	34
2C	05/18/04	06/21/04	35
3A	10/03/04	11/08/04	37
3B	02/17/05	03/24/05	36
3C	05/20/05	06/23/05	35
3D	10/21/05	11/24/05	35
3E	02/22/06	03/27/06	34
3F	05/24/06	06/26/06	33
3G	10/25/06	11/27/06	34
3H	03/12/07	04/14/07	34
3I	10/02/07	11/05/07	37
3J	02/17/08	03/21/08	34

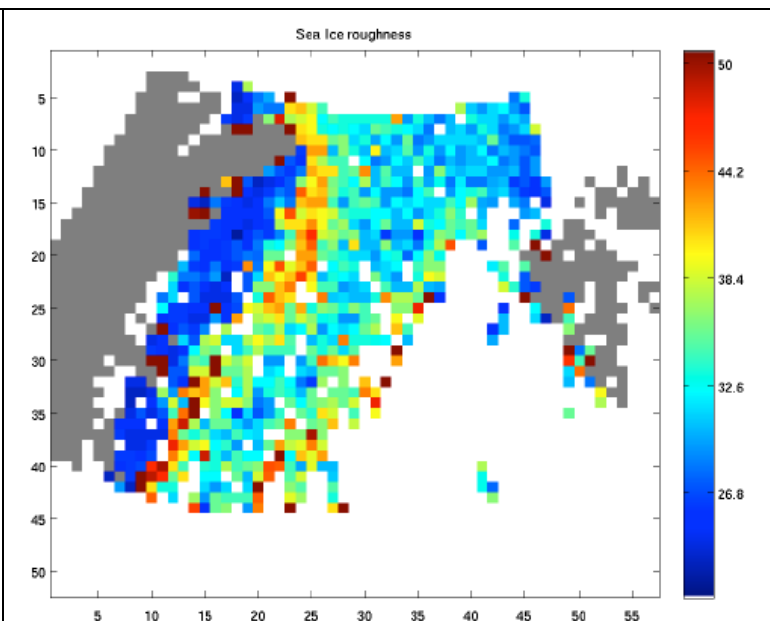


Figure 4.1: Sea surface roughness of the sea ice in 20 km bins in the Fram Strait. The smooth fast ice near Greenland is clearly visible as a blue band on the left. The roughest ice is multiyear ice drifting southwards from the north of Greenland.

The most important parameter calculated from the IceSat data are summarized in Table 4.2. It includes the standard deviation between the expected Gaussian waveform echo and the actual received waveform [Korn, 2009]. The Gaussian waveform is what would be expected from a smooth surface of sea ice, so a large deviation from this would imply a surface that is not a smooth sheet of ice. Surface roughness is a measure of the ice roughness, however it seems like the *i_sealvar* might have some additional information.

Ice thickness retrieval from the IceSat data has been tested, using five data sets (2003 – 2007). The filtering method proposed by Kwok (2006) has been used. The ArcGP geoid has been used as height reference and 25 km running mean has been applied on the profile data. The averaged lowest 2 % of data in each 25km segment has been used as sea surface reference. Assumptions on snow and ice properties have been made, and the isostatic equilibrium hypothesis has been used to derive thickness from freeboard estimates. A section of data at 79° N from 15° W to 3° E has been extracted. The preliminary results of the ice thickness retrieval at 79° N are presented in Fig. 4.2.

Table 4.2: IceSat parameters that have been studied, with a short explanation

i_gval_rcv	Gain used for received pulse.
i_SealceVar	Standard deviation of the sea ice Gaussian fit
i_reflctUncorr	Reflectivity not corrected for atmospheric effects
i_numPk	Number of peaks found in return
i_RufSealce	Sea Ice roughness
i_elev	Sea Ice Surface elevation

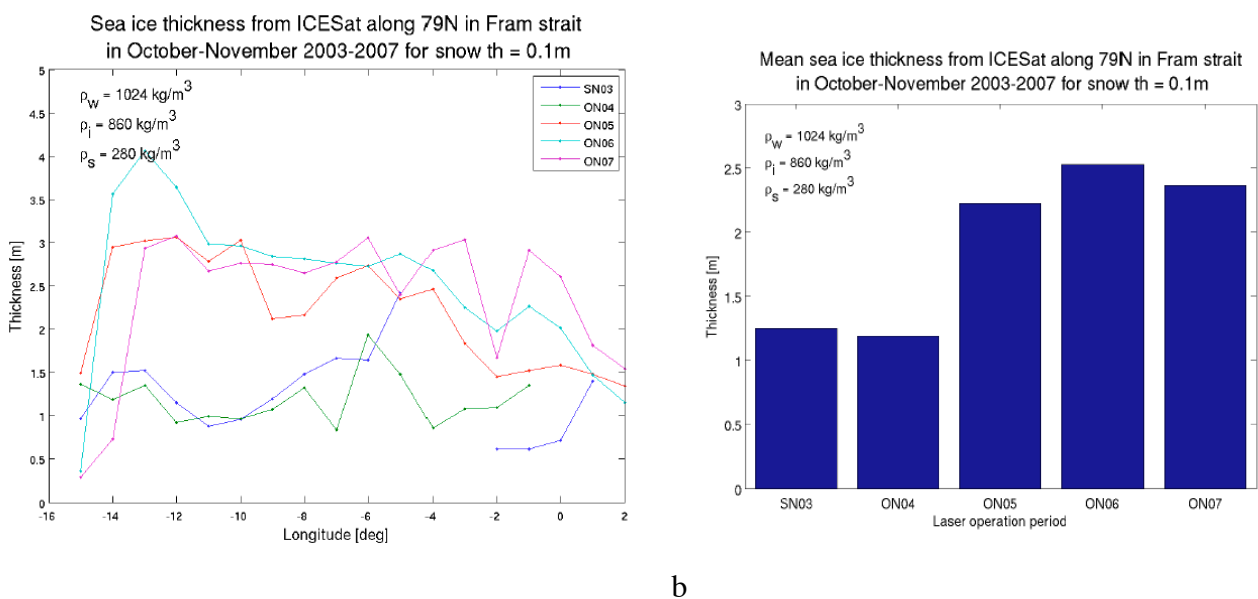


Figure 4.2. (a) profiles of ice thickness across 79 N retrieved from IceSat data for five different periods; (b) histogram of mean ice thickness retrieved from IceSat data for the five periods.

The results of the ice thickness retrievals are not yet discussed, but there is a need to compare with other data and to assess the assumptions made in the isostatic equilibrium hypothesis about snow and ice properties. Further work will include more sea ice products in analysis, i.e. AMSR-E snow depth and ice concentration. The ice area flux from SAR provided by NERSC will be combined with calculated ice thickness to estimate volume flux across 79N in Fram Strait. An example of ice volume flux calculation using IceSat thickness combined with ice area flux is shown in Table 4.3.

Table 4.3 Initial estimates of ice volume flux

Period: October-November	2004	2005	2006	2007
IceSat thickness (m) from Fig 4.2 b	1.18	2.23	2.53	2.35
SAR-base ice area flux (1000 km ²)	45	90	120	128
Volume flux (km ³ per day)	1.5	5.9	9.2	9.1
Volume flux (km ³ per day) by Spreen et al. (2009)	4.5	8.5	7.5	10.0

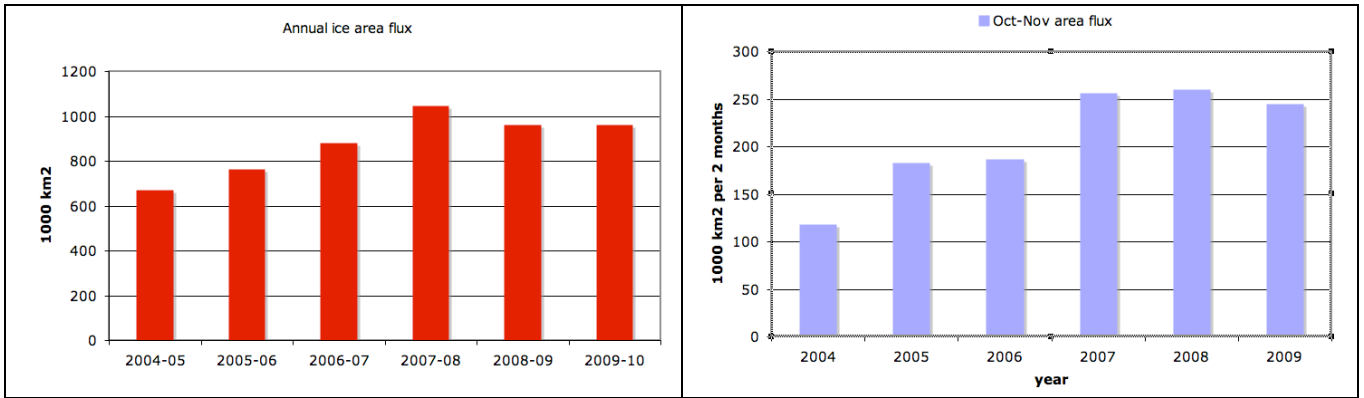


Figure 4.3. Ice area flux derived from SAR image from 2004 to 2010. Left: annual mean area flux. Right: Area flux for October and November, coinciding with the thickness measurements from IceSat. Note that the period of ice area flux in Table 4.3 is about 5 weeks while the estimates in the diagramme is for the whole of October and November.

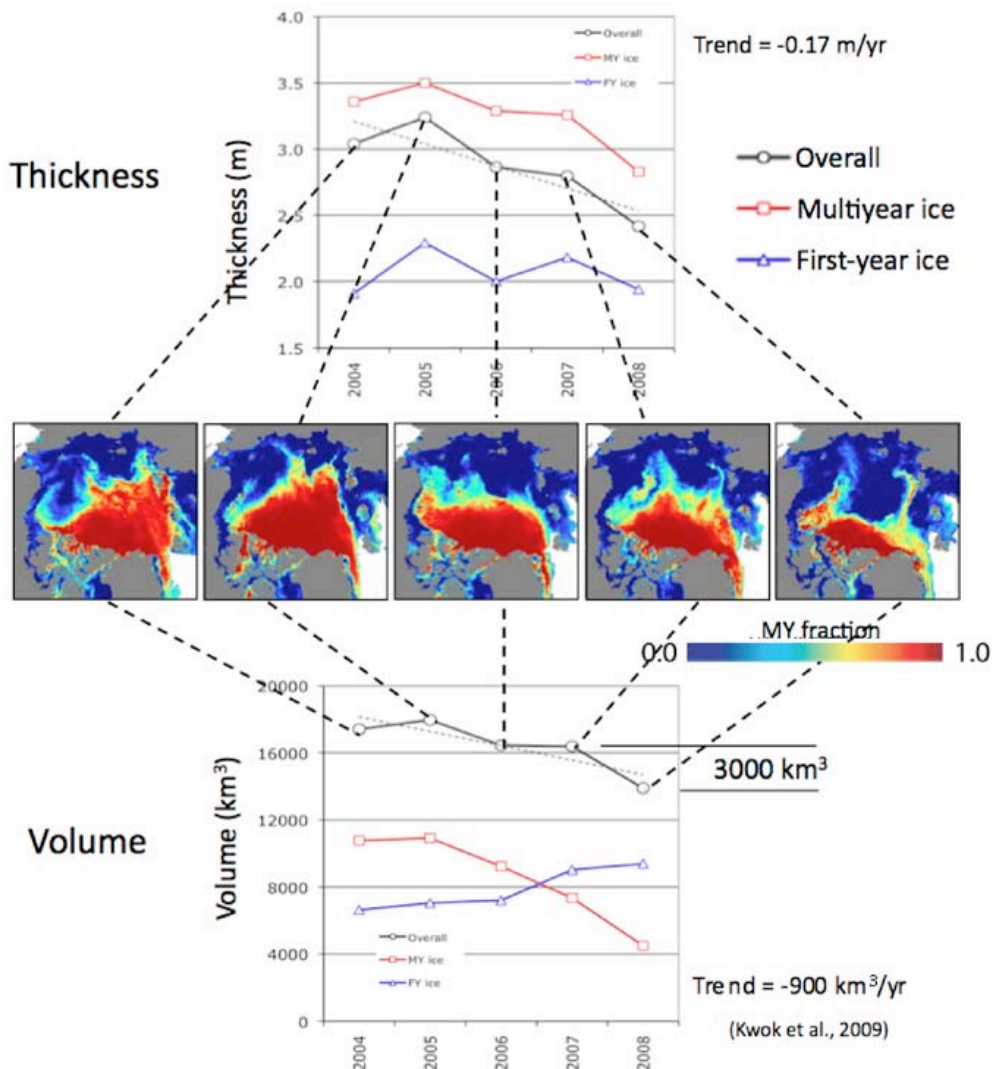


Figure 4.4. Changes in ice thickness and volume in the Arctic based on thickness data from IceSat and area data from scatterometer (Kwok et al., 2009)

By comparing the results in Fig 4.3 and 4.4 it appears that the reduction in ice volume from 2004 to 2007 for multiyear ice is consistent with increasing volume flux in October – November, when the ice is mainly multiyear. More studies are needed to study changes in thickness, area and fluxes. More work will be done to estimate ice thickness in areas where validation data is available, especially from field work during the IPY campaigns. Further work will be done to analyze IceSat data in the Fram Strait to study the laser signal for different ice types and water surfaces, and to validate freeboard and ice thickness estimates with in situ data.

First look at CryoSat data

The Cryosat SIRAL data have been available since 15 July 2010 as level 1b data over sea-ice in DBL-files. The two daily (ascending and descending) tracks covering the Fram Strait (area 78N - 84N, 15W - 10E) have been downloaded and processing has been tested. Ascending time is near 00z, descending near 12z, this will slowly change since the orbit is not sun-synchronous. Processing is now made to a greytone-signal-power image, with signal-time (=surface-height) in x, and alongtrack-position in y (as was done with ASIRAS in 2008). Calibrated position is given in the DBL-file, work on calibrating signal-time (=surface-height) and interpreting signal-power is planned. Resolution is 300m in position (y). The array of signal-times has 128 values (x), defining the resolution of surface-height. The received radar signal (average power-echo) is coded in 2 bytes and conversion factors to Watts are given. Processed tracks of length up to 600km will be compared with available ASAR WSM images. When available, also optical images can be used in comparison. Shape of the signal-power versus signal-time profile is supposed to give information about surface roughness, with sharp and strong power peak for smooth surface (new ice, calm water) and weaker power in broader shape for rough surface (thick ice, rough water). Due to some processing errors in the L1B data product, reported at the CryoSat Workshop at ESRIN 1 – 3 February 2011, further analysis is postponed until a new version of L1b data are available.

WP5: Plan for post-launch experiments

WP5: Planning of CryoSat post-launch experiment

Conduction of CryoSat Cal/Val-relevant field activities 2010

As a part of the new Center for Ice, Climate and Ecosystems (ICE) at the Norwegian Polar Institute and its flagship project "ICE-Fluxes", in autumn 2009 the NPI ordered a so called "EM-bird", a helicopter-borne instrument for ice thickness transects. The instrument was delivered in autumn 2010 and will be used first in two cruises with KV "Svalbard" and RV "Lance" in spring 2011. In August and September 2010, EM bird measurements and experience could be collected through collaboration with University of Alberta (C. Haas) on two sea ice cruises, one to the sea ice north of Svalbard, and the second to the Fram Strait at 79 N. At both cruises snow and sea ice parameters relevant for CryoSat Cal/Val were obtained..

UNIS have had a field experiment with RV Lance in April 2010 to collect more sea ice data for validation of CryoSat retrievals. The experiment took place northwest of Svalbard where there will be dense coverage of CryoSat orbits. The area contains both multiyear ice, firstyear ice, leads, ridges and open water. The area is therefore well suited for a post-launch experiment. The main post-launch experiment for CryoSat is expected to take place in the spring of 2011.

An EM31- ice ground conductivity meter was purchased by UNIS from Geonics as planned. Unfortunately, due to delayed delivery from Geonics this ice thickness instrument did not arrive in time for the winter sea ice campaign and could not be tested in the field in 2009. A higher cost from Geonics and a switch in the EUR and USD currency, made the EM31 more costly than

originally written in the budget. Funding for the helicopter campaign had to be used in order to purchase this key instrument for the 2010 field campaign.

In addition to in situ and helicopter data, it is also necessary to conduct airborne campaigns to collect data over larger areas, similar to what has been done in previous pre-launch campaigns. The different observing scales from satellite, fixed-wing aircraft, helicopter and in situ data requires that data are collected at all these scales.

Plan for 2011

During early 2011, the first large post-launch calibration and validation campaign for CryoSat-2 (CryoVex 2011) is planned in several places in the Arctic (Pearson and Wooding, 2011). In situ sea ice work led by the Norwegian Polar Institute in spring 2011 is a part of the CryoVEX 2011 Campaign Implementation Plan. During two cruises in spring 2011, NPI plans to conduct several helicopter flights, with the new NPI EM bird, along CryoSat-2 tracks within closest possible overflight time. An EM bird is a device for measuring the total sea ice thickness from helicopter or aircraft over long transects (Haas et al. 2009). Similar, close to simultaneous, flights were done in August and September 2010 from Lance, using an EM bird from the University of Alberta, Canada (collaboration with Christian Haas and Justin Beckers). Based on this experience, we anticipate realistic line helicopter transect lengths of about 50-100 km. To keep control of ice drift between and during CryoSat overflight and helicopter measurements, we will deploy GPS drifters along the lines. Helicopter flight lines will be coordinated with the planned aircraft campaigns (Twin Otter with ASIRAS and Polar 5).

For each of the aircraft overflights, helicopter transects along the same lines will be performed (weather permitting), and corresponding in situ measurements on ice floes will be conducted. During the KV Svalbard cruise, we plan five longer helicopter transects along CryoSat overpass lines, combined with in situ snow and sea ice work. Ground measurements (from ship and helicopter) on several ice floe stations include electromagnetics (Geonics EM31, one NPI instrument and one UNIS instrument), drillings, and sampling. This will complement the airborne work, giving us information on the snow cover (thickness distribution and density, see e.g. Forsström et al. 2011), as well as on snow and ice properties.

SAR satellite images (Radarsat and Envisat), combined with high-resolution optical images will be used classifying the sea ice in the regions where aircraft surveys and in situ measurements are collected. The satellite data will be used to quantify which ice types are representative/most abundant and for estimation of ice drift.

UNIS will have a field experiment with RV Lance in April 2010 to collect more sea ice data for validation of CryoSat retrievals. The experiment will take place northwest of Svalbard where there will be dense coverage of CryoSat orbits. The area contains both multiyear ice, firstyear ice, leads, ridges and open water. The area is therefore well suited for a post-launch experiment. In case CryoSat data will be available in April 2010, the experiment can serve as a post-launch campaign. The main post-launch experiment for CryoSat is expected to take place in the spring of 2011.

An EM31- ice ground conductivity meter was purchased from Geonics as planned. Unfortunately, due to delayed delivery from Geonics this ice thickness instrument did not arrive in time for the winter sea ice campaign and could not be tested in the field in 2009. A higher cost from Geonics and a switch in the EUR and USD currency, made the EM31 more costly than originally written in the budget. Funding for the helicopter campaign had to be used in order to purchase this key instrument for the 2010 field campaign.

In addition to in situ and helicopter data, it is also necessary to conduct airborne campaigns to collect data over larger areas, similar to what has been done in previous pre-launch campaigns. The different observing scales from satellite, fixed-wing aircraft, helicopter and in situ data requires that data are collected at all these scales.

WP6: Workshop/conference on CryoSat2 sea ice data

Meetings and publication activities

At the CVRT meeting in Reykjavik, Iceland, in June 2009, the last results from this project were presented by S. Gerland (NPI) and J. Wåhlin (NERSC). The CryoSat campaign and related Cal/Val work was mentioned in several presentations to the public. A report (S. Forsström and S. Gerland: Report on thicknesses and densities of sea ice and snow from historical and recent field data) was delivered to ESA and NSC in February 2009 (1st deliverable in the projects WP1). A scientific paper on this content (Forsström et al. 2011) was recently published in the *Annals of Glaciology* volume (57) for the Sea Ice Symposium of the International Glaciological Society (Tromsø, May/June 2010). NERSC has published a paper on analysis of ice and snow data from the Sever expeditions in *The Cryosphere* (Alexandrov et al. 2010).

The CryoSat workshop at ESRIN 01-03 February 2011 provided status on CryoSat operation and data delivery. The level 1b data over sea ice has to be reprocessed before level 2 data can be provided. A CryoSat workshop in Norway is planned to take place in second half of 2011 or 2012 when data and results of on sea ice thickness retrievals are available.

References

- Ackley, S.F., W.D. Hibler, III, F.K. Kugzruk, A. Kovacs and W.F. Weeks (1976): Thickness and roughness variations of Arctic multiyear sea ice. *CRREL Rep.*, 76-18.
- Alexandrov, V., S. Sandven, J. Wåhlin, and O. M. Johannessen (2010): The relation between sea ice thickness and freeboard in the Arctic. *The Cryosphere* 4, 373-380. (www.the-cryosphere.net/4/373/2010/) (doi:10.5194/tc-4-1-2010).
- Cullen, R. "ASIRAS Product Description, Issue 2.5". Cryosat project document, ESTEC, 9. Sep.2007.
- Cullen, R. "CryoVEx Airborne Data Products Description." Issue 2.6.1. ESTEC 06. Jan 2010. ([ftp.cryosat.esa.int](ftp://cryosat.esa.int) in/from_estec/Documents/Product_Descriptions)
- Emery, William J. and Richard E Thomson (2004). *Data analysis Methods in Physical Oceanography*, Elsevier, 2.edition
- Forsström, S., and S. Gerland (2009): Report on thicknesses and densities of sea ice and snow from historical and recent field data. Internal delivery report, Norwegian Polar Institute, 29 pages.
- Forsström, S., Gerland, S. & Pedersen, C.A. (2011): Sea ice and snow densities and hydrostatic equilibrium assumption from in situ measurements in Fram Strait, Barents Sea and Svalbard coast. *Annals of Glaciology* 57 (52), pp. 261-270.

Geonics Ltd., EM31-ICE Operating instructions, Geonics Ltd

Gerland, S., A.H.H. Renner (2007), Sea ice mass balance monitoring in an Arctic fjord, *Annals of Glaciology*, Vol. 46, pp. 435-442.

Gerland, S., R. Hall (2006), Variability of fast ice thickness in Spitsbergen fjords. *Annals of Glaciology*, Vol. 44, pp. 231-239.

Gerland, S., Haas, C., Hall, R., Holfort, J., Hansen, E., Løyning, T.B., and Renner, A. (2006), Spring sea ice thickness in the western Fram Strait: Preliminary results. In: P. Wadhams & G. Amanatidis (eds.): *Arctic Sea Ice Thickness: Past, Present and Future*. Climate Change and Natural Hazards Series 10, EUR22416, European Commission, Brussels, 2006, 293 pages, pp. 158-164.

Haas, Christian, Sebastian Gerland, Hajo Eicen and Heinz Miller (1997). Comparison of sea-ice thickness measurements under summer and winter conditions in the Arctic using a small electromagnetic induction device, *Geophysics* vol. 62.No.3.

Haas, C., J. Haapala, S. Hansson, L. Rabenstein, E. Rinne, J. Wilkinson. CryoVEx 2006 Field Report. Alfred Wegener Institute for Polar and Marine Research, November 2006, 38 pp.

Haas, C, S. Hanson, S. Hendricks: CryoVEx 2008 Field report of in-situ measurements, 2008

Hvidegaard, S. M., R. Forsberg V. Helm, S. Hendricks, H. Skourup, L. Stenseng, S. Hanson, and C. Haas. CryoVEx 2008 Final Report. Danish National Space Institute, Danish Technical University, Technical Report 2/2009, ISBN 978-87-92477-040, <http://www.space.dtu.dk>

Kwok, R., G. F. Cunningham, M. Wensnahan, I. Rigor, H. J. Zwally, and D. Yi (2009), Thinning and volume loss of the Arctic Ocean sea ice cover: 2003–2008, *J. Geophys. Res.*, 114, C07005, doi:10.1029/2009JC005312.

Kwok, R., and G. F. Cunningham (2008), ICESat over Arctic sea ice: Estimation of snow depth and ice thickness, *J. Geophys. Res.*, 113, C08010, doi:10.1029/2008JC004753.

Kwok, R., G. F. Cunningham, H. J. Zwally, and D. Yi (2007), Ice, Cloud, and land Elevation Satellite (ICESat) over Arctic sea ice: Retrieval of freeboard, *J. Geophys. Res.*, 112, C12013, doi:10.1029/2006JC003978

Lepparanta, M. (1991). A review of analytical models of sea-ice growth, *Canadian meteorological and oceanographical society*.

Loshchilov, V.S. (1964), Snow cover on the ice of the central Arctic. *Problemy Arktiki I Antarktiki*, 17, 36-45 [in Russian].

Leuschen, C. J., and R. K. Raney (2006), Initial results of data collected by the JHU/APL D2P radar altimeter over land- and sea-ice, *Johns Hopkins APL Tech. Dig.*, 26, 114– 122.

National Snow and Ice Data Center. 2004. Morphometric characteristics of ice and snow in the Arctic Basin: aircraft landing observations from the Former Soviet Union, 1928-1989. Compiled by I.P. Romanov. Boulder, CO: National Snow and Ice Data Center. Digital media.

Pearson, T. and M. Wooding. CryoVEx 2011 Campaign Implementation Plan, Draft v0.4, January 2011.

Romanov, I.P. (1995) *Atlas of Ice and Snow of the Arctic Basin and Siberian Shelf Seas*, edited by A. Tunik, Backbone Publishing, Elmwood Park, USA, 277 pp

- Sandven S. et al., CRYOSAT sea ice calibration/validation studies. NERSC Technical report no. 257, June 2005, 50 pp.
- Spreen, G. S. Kern, D. Stammer, R. Forsberg and J. Haarpaintner. Satellite-based estimates of sea ice volume flux through Fram Strait. *Annals of Glaciology*, 44, 2006, pp 321- 328.
- Stenseng, L., S. M. Hvidegaard, H. Skourup, R. Forsberg, C. J. Andersen, S. Hanson, R. Cullen, and V. Helm. Airborne Lidar and Radar Measurements In and Around Greenland (CryoVEx 2006). ESA CONTRACT NO19601/05/NL/GS, Danish National Space Center, Technical report 9/2007, 148 pp.
- Thomas, David N. and Gerhard S. Dieckmann (2003). SEA ICE and introduction to its Physics, Chemistry, Biology and Geology. Blackwell Science Ltd.
- Timco, G.W., and Frederking, R.M.W.: A review of sea ice density, *Cold Reg. Sci. Technol.*, 24, 1-6, 1996.
- Vinje, T. and Ø. Finnekåsa (1986): The ice transport through the Fram Strait. *Nor. Polarinst. Skr.* 186, 1–39.
- Vinje, T., N. Nordlund and A. S. Kvambekk. 1998. Monitoring ice thickness in Fram Strait. *J. Geophys. Res.*, **103**(C5), 10,437–10,450.
- Warren, S.G., I.G. Rigor, N. Untersteiner, V.F. Radionov, N.N. Bryazgin, Y.I. Aleksandrov, and R. Colony (1999), Snow depth on Arctic Sea Ice, *J. Clim.*, 12, 1814-1829.

Appendix: Processing of ASIRAS and ALS data

A1. ASIRAS 2008 reprocessed data processing

Examples of ASIRAS data have been selected and downloaded from *ftp.cryosat.esa.int* using */from_estec/CryoVEx_Processed_Data_Sets/CryoVEx/Reprocessed/CryoVEx_2008/level_11b/*

ASIRAS file naming is: AS3OAx ASIWL1B0402<start datetime>_<stop datetime>_0001.DBL where:

AS3 = ASiras platform 3 (Twin Otter), O = Operational, Axx = Profile number xx, ASIWL1B = Windowed LAM-A (=Low Alt. Mode (LAM) format with reduced window size of 256 samples/profile), 0402 = Software version 04.02, 001.DBL = Processed data version 001.

File data structure is found in table 3-21 in Cullen (2010) (Earlier format had 1024 samples/profile.)

Data from the ASIRAS flights over the MY/FY sea ice boundary situated at 83.341N were downloaded. These data files were uncompressed with the following number of rec"s and lines.

Profile no	rec"s	#lines
A27	849	16980
A36	989	19780

The layout for Dataset A27 is (#bytes in paranthesis): MPH(1247) +SPH(1112) + 5 DSD(280) +849 Datarec(16 660).

Here:

MPH = Main Product Header, in Table 3-15

SPH = Specific Product Header, in Table 3-16

DSD = Data Set Description, in Table following SPH.

Total filesize = 3759 + 849 * 16 660 = 14 148 099 by.

The format for ASI_LAM_W_L1B (ASIWL1B) is described in Table 3-21 in the ASIRAS Product Description(Cullen, 2007). The structure is (#bytes in paranthesis):

20 Time&Orb.group(84) + 20 Meas.group(94) + Correc.group(64) + Avg.Wavef.(512+44) + 20 Multilook.Wavef.(624).

Total size = 4 180 + 12 480 = 16 660 by.

Each multilook waveform ("line") has 256 samples ("range bins") of 2by unsigned integer, followed by 8by Scalefactors, 4by Echo/Flags, 100by Beam param. Total size = 2 * 512 + 112 = 624 by.

Processing DBL file (ASraw) to profile images

- a) Remove headerbytes and all bytes before the 20 waveform data:
>bin2gop ASraw ASraw.imf <# records> 12480 3759 4180 0

- b) Convert to one waveform (256 bins a 16bit) per line:
 >bin2gop ASraw.imf AS@.imf <# lines> 512 12480 0 112 @= Dataset
- c) Convert AS@.imf file to imf-file with 8-bit data:
 >rfile2e.y (on Nansen, after June 08) with:
- Infile: AS@.imf rec.size = 512 by
 - Outfile: AS@x.imf rec.size = 256 where x =b, c, (waveforms a 256 by)
 - A gain of approx. 0.01 is be used to avoids saturation (data>255) of the data.

A2. ALS 2008 data processing

AWI Laser Scanner (ALS) files have been selected and downloaded from *ftp.cryosat.esa.int* in:
 /from_estec/CryoVEx_Processed_Data_Sets/CryoVEx/CryoVEX_2008/ALS/

File data structure of these ALS AWI Level 1b data is given in Cullen (2010) chapter 3.2.12.2. Data corresponding to ASIRAS flights over the FY/MY sea ice boundary situated at 83.341N were downloaded:

A27 02.May 2008 21:15:22 – 21:25:03z 83.3084N, 65.170W – 83.6582N, 65.169W A36
 02.May 2008 22:37:06 – 22:47:02z 83.4868N, 65.169W – 83.1044N, 65.169W

These data files were uncompressed with the following number of scanlines.

<u>Profile</u>	<u>Scanlines</u>	<u>Datapoints/line</u>
A27	4722	251

The layout for A27 with 4722 scanlines is (#bytes in paranthesis):
 Header(36by) +4722 Timestamps(4by) + 4722 DEM-records(4 * 251 *8by).
 Total filesize = 18 924 + 4722 * 4 *251 * 8 = 37 946 028 by.
 4 bytes are use for each timestamp, 8 bytes for each value (val) of the 4 parameters in DEM.

The arrangement of the 251 cross-track values in each of the 4722 DEM records is:

251 Time(8by) + 251 Lat.(8by) + 251 Lon.(8by) + 251 surf.elev..(8by)
 Total size = 8032 by.

Processing ALS file (ALSraw) for plotting

- a) Remove headerbytes :
 >bin2gop ALSraw ALS.imf <# scanlines> 8032 18924 0 0
- b) Convert ALS.imf file to binary image with 8-bit elevation data:
 >rals.y (on Nansen) with:
- Infile: ALS.imf
 - First rec.: 1758 for surface elevation, (= 1+ 8032 /8 + 3 * 251)
 - 5-groups-no. start: e.g. =10. Choose start-scanline no.
 - No.of col.: e.g. =40. Choose # of scanlines.
 - Give conversion of val to 8-bits in iv=(val-a)*b, e.g.: a, b= 19.5, 100
 - Outfile: ALS.dat